J. Fluid Mech. (1992), *vol.* 234, *pp.* 329–360
Printed in Great Britain

The three-dimensional turbulent boundary layer near a plane of symmetry

By A. T. DEGANI[1], F. T. SMITH[2] AND J. D. A. WALKER[1]

[1] Department of Mechanical Engineering and Mechanics, Lehigh University, Bethlehem, PA 18015, USA

[2] Department of Mathematics, University College, London WC1E 6BT, UK

(Received 25 January 1991 and in revised form 16 July 1991)

The asymptotic structure of the three-dimensional turbulent boundary layer near a plane of symmetry is considered in the limit of large Reynolds number. A self-consistent two-layer structure is shown to exist wherein the streamwise velocity is brought to rest through an outer defect layer and an inner wall layer in a manner similar to that in two-dimensional boundary layers. The cross-stream velocity distribution is more complex and two terms in the asymptotic expansion are required to yield a complete profile which is shown to exhibit a logarithmic region. The flow in the inner wall layer is demonstrated to be collateral to leading order; pressure-gradient effects are formally of higher order but can cause the velocity profile to skew substantially near the wall at the large but finite Reynolds numbers encountered in practice. The governing set of ordinary differential equations describing a self-similar flow is derived. The calculated numerical solutions of these equations are matched asymptotically to an inner wall-layer solution and the results show trends that are consistent with experimental observations.

1. Introduction

Most boundary-layer flows in engineering applications are turbulent and three-dimensional. However, until relatively recent times, a considerable majority of theoretical and experimental studies have dealt with the simpler two-dimensional boundary layer for which results have become well-established over the past few decades (at least for nominally steady flows). Unfortunately, the body of established information for three-dimensional boundary layers lags far behind the two-dimensional case. A common theme has been to infer the nature of three-dimensional boundary layers based on *ad hoc* extensions of the two-dimensional theory. In particular, a number of law-of-the-wall models have been proposed, but in a critical review (Pierce, McAllister & Tennant 1983) it is concluded that none of the models is satisfactory. There are several critical issues which have been controversial and involve seemingly conflicting experimental evidence. These issues will be discussed subsequently, but at this stage it is worthwhile to describe the general features of the three-dimensional boundary layer.

Three-dimensional boundary layers are most conveniently described in a streamline coordinate system as shown schematically in figure 1. The velocity vector, which is aligned in the direction tangential to the external streamline at the boundary-layer edge, tends to rotate in the direction of decreasing cross-stream pressure gradient. Hence, as the wall is approached, the magnitude of the cross-

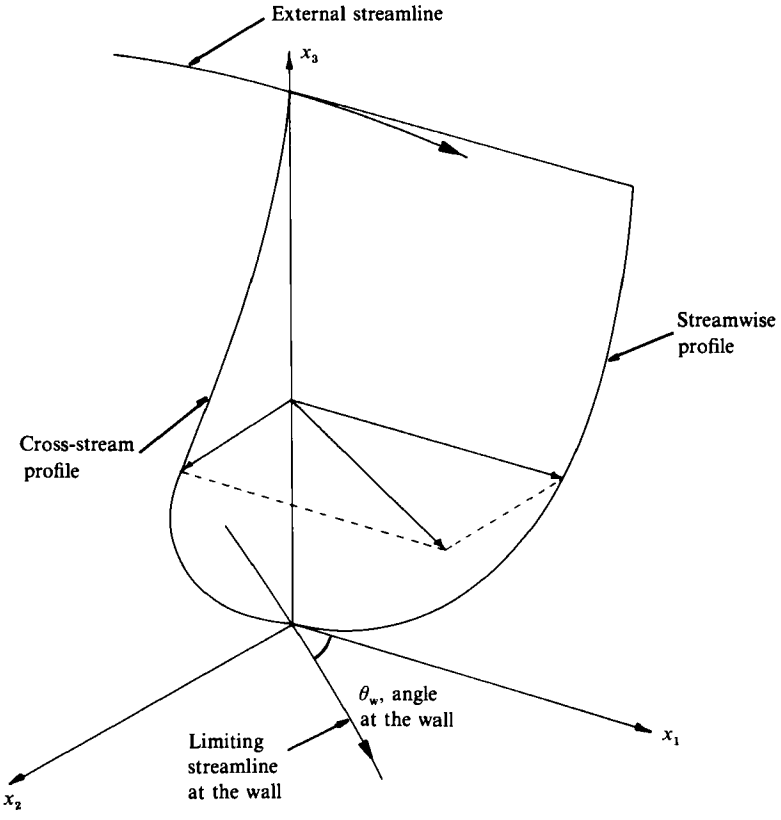

FIGURE 1. Schematic of a three-dimensional turbulent boundary-layer velocity profile.

stream velocity increases from zero at the boundary-layer edge, reaches a maximum value, and then decreases back to zero at the wall in order to satisfy the no-slip condition. In contrast, the behaviour of the streamwise velocity is qualitatively similar to that in two-dimensional boundary layers. Both the streamwise and cross-stream velocities are zero at the wall and the tangent to the limiting streamline at the wall is determined by the direction of the wall shear stress vector. In general, the angle between the tangents to the external streamline and the limiting streamline at the wall is non-zero; therefore, as the breadth of the boundary layer is traversed, the velocity vector rotates through what will be referred to as the skew angle at the wall. Similarly, the total shear stress vector tends to rotate away from its direction at the wall with increasing distance from the surface.

The three-dimensional turbulent boundary layer is generally believed to be double-structured, consisting of a relatively thick outer layer and an inner wall layer. Here the term 'wall layer' denotes the region close to the wall where the turbulent and viscous shear stresses are of comparable magnitude. The nature of the flow in the wall layer of a three-dimensional boundary layer has been the subject of some controversy. The earlier experiments of Johnston (1960) and Hornung & Joubert (1963) seemed to suggest that the flow near the wall is collateral and in the direction of the wall shear stress. Here the terminology 'collateral' implies that below a certain value of y^+, the local velocity is aligned in the direction of the shear stress at the wall. Johnston (1960) claimed that this region extended from the wall to about $y^+ = 15$, but Hornung & Joubert (1963) later stated that this region could extend to as much

as $y^+ = 150$. A number of subsequent experiments (Prahlad 1973; Fernholz & Vagt 1981) indicated that a substantial skewing of the velocity profile could occur in the region very close to the wall. In a review article, Johnston (1976), citing additional experimental data, remarked that about as much as half the total skewing of the velocity profile could occur from $y^+ = 0$ to $y^+ = 100$. However, other experimental data (Francis & Pierce 1967; Klinksiek & Pierce 1970) seemed to suggest that the flow close to the wall is indeed collateral. Unfortunately, measured profile data in the near-wall region of a three-dimensional boundary layer are rare. Evidently the issue of whether the flow is collateral or not in the region close to the wall has not been resolved by observation.

Experimental data (Klinksiek & Pierce 1970; Pierce & Zimmerman 1973; Van den Berg *et al.* 1975; Hebbar & Melnik 1978) indicate that the streamwise velocity profile has a logarithmic zone, the extent of which is comparable to that in two-dimensional boundary layers. This has led some authors (e.g. Chandrasekhar & Swamy 1976) to speculate on the existence of a similar region for the cross-stream velocity. A few law-of-the-wall models have been proposed which assume a logarithmic profile for the cross-stream velocity, but there appears to be no clearly supportive experimental corroboration. Another issue of some note is the choice of the appropriate velocity scale in the wall layer. In two-dimensional boundary layers, the obvious scale is the friction velocity u_τ, the square of which is defined as the wall shear stress divided by the density. However, in three-dimensional boundary layers, there are a number of possibilities, some of which have been discussed by Pierce *et al.* (1983) who conclude that there is no clear choice for the wall-layer velocity scale.

One approach to constructing a three-dimensional 'law of the wall' is to determine the asymptotic structure and the scaling laws for the three-dimensional turbulent flow equations in the limit of large Reynolds number. The asymptotic structure for two-dimensional boundary layers has been developed by a number of authors (Yajnik 1970; Mellor 1972; Fendell 1972), with results that are consistent with Clauser's (1954, 1956) synthesis of experimental data. However, analysis of the three-dimensional problem has been restricted to a recent study by Goldberg & Reshotko (1984) who extended Mellor's (1972) work to three dimensions. They concluded that in the inner wall layer, the flow is collateral and that the pressure-gradient and convection terms are negligible through three leading-order terms; although their analysis is valid in the limit of infinite Reynolds number, the result of collateral flow throughout the extent of the wall layer does not appear to be corroborated by experimental data at the Reynolds numbers encountered in practice. In Goldberg & Reshotko's (1984) asymptotic expansions of the velocity, the form of the gauge functions was assumed *a priori* and unfortunately it is very difficult to account for the effects of pressure gradient in the wall layer even when such an analysis is extended to higher orders. However, it is widely believed (see, for example, Nash & Patel 1972) that the pressure gradient is responsible for skewing of the velocity profile in the wall layer. Earlier, Van den Berg (1975) attempted to reconcile experimental data with analytical results by including the effects of both pressure gradient and convection on the flow in the wall layer. With the x-axis of a local Cartesian coordinate system aligned along the shear stress direction at the wall and z measuring spanwise distance, an integration of the x- and z-momentum equations was carried out by neglecting the spanwise convection terms and assuming a logarithmic asymptotic form (for large y^+) for the x-direction velocity. Although Van den Berg's (1975) approach accounts for some of the effects of pressure gradient and convection in the wall layer, it is limited in its applicability because the proposed

inner-layer solutions were not matched to an outer-layer solution and the means of accomplishing this match were not addressed. Furthermore, the velocity skew angle at the wall was assumed known for a given external flow condition. Recently Barnwell (1991) has also indicated a procedure for incorporating pressure-gradient effects near the surface in a compressible flow. It will be shown in the present study that the velocity skew angle is dependent on the Reynolds number and must be determined as part of the boundary-layer solution.

2. Motivation and objectives

It is evident from the foregoing brief survey of research progress in three-dimensional turbulent boundary layers that there are a number of important fundamental issues. An asymptotic analysis was carried out in this study since it has the potential of systematically addressing and resolving several aspects. In particular, the following specific points are of interest:

(*a*) In practical flows of interest, the inner layer is believed to extend from the wall to about $y^+ = 50 \sim 100$. Although a number of researchers have observed what appears to be collateral flow in the near-wall region, none (with the exception of Hornung & Joubert 1963) have claimed the flow to be collateral all the way to $y^+ = 100$. Since the pressure gradient is believed to cause skewing in the wall layer, the asymptotic analysis should be capable of quantitatively determining the influence of the pressure gradient on the inner flow at Reynolds numbers encountered in practice. The present study is in the spirit of Fendell's (1972) analysis, where the appropriate asymptotic expansions are indicated during the course of the analysis (see also Van Dyke 1964, p. 93); this is in contrast to the studies of Mellor (1972) and Goldberg & Reshotko (1984) where the form of the gauge functions was assumed *a priori*.

(*b*) Unlike the streamwise velocity profile, the existence of a logarithmic zone for the cross-stream profile has not been established. Furthermore, no rational model has been proposed which describes the manner in which the cross-stream velocity increases from zero at the boundary-layer edge to a maximum value within the boundary layer, and then adjusts back to zero to satisfy the no-slip condition at the wall. The present analysis will show that the characteristic 'bulge' in the cross-stream velocity is a natural consequence of its asymptotic form in the matching region between the wall and outer layers.

(*c*) Although an asymptotic analysis cannot determine a specific closure (such as an eddy-viscosity model) throughout the boundary layer, it can suggest the correct scaling laws and constrain the possible forms allowable for asymptotic consistency with the flow structure; in this manner, a basis is established to assess the possible extensions of various two-dimensional algebraic eddy-viscosity models (such as the Cebeci–Smith 1974 and Baldwin–Lomax 1978 models) to three dimensions (see, for example, Cebeci 1975; Wie & DeJarnette 1988).

(*d*) Through an asymptotic analysis of the governing equations, it is possible to determine quantitatively the dependence of the skew angle at the wall on the Reynolds number, an issue which has not been discussed previously in the literature.

In their asymptotic analysis of the full three-dimensional equations, Goldberg & Reshotko (1984) worked in Cartesian coordinates and assumed that the mainstream velocity had two orthogonal non-zero components. The velocity in the two directions was treated in the same fashion, thus yielding a two-dimensional 'law of the wall' for both directions. However, such an analysis is possible only when each component of the outer-layer velocity can be expressed as a sum of a *non-zero* mainstream velocity

and a defect function. The approach fails when either of the two components of the external velocity is zero. The issues involved in the analysis of the full three-dimensional equations are complex and involve a number of subtle points. Consequently, as a first step, the simplest possible three-dimensional turbulent boundary-layer flow is considered here, namely the flow in a plane of symmetry, where in general the flow develops independent of the rest of the boundary layer. The advantage of such an approach is that, to leading order, the streamwise momentum equation can be analysed independently of the cross-stream equation. Once the asymptotic structure of the streamwise momentum equation is established, the cross-stream equation can then be addressed. In the plane of symmetry, the cross-stream velocity and the total stress are both identically zero; however, their cross-stream gradients are non-zero, and the asymptotic expansions are developed for these quantities. The resulting solutions are the first terms in a Taylor series expansion about the plane of symmetry, and, therefore, may be used to infer the flow behaviour near the plane of symmetry.

In view of the above motivation, the objectives of the present study are as follows:

(i) to establish the asymptotic structure of the three-dimensional turbulent boundary layer in a plane of symmetry by developing a self-consistent set of scaling laws which are also compatible with experimental observations; and

(ii) to obtain sets of self-similar velocity and shear stress profiles.

Although the self-similar profiles represent a subset of more general types of flow, they are useful in developing an understanding of the essential structural features of a three-dimensional turbulent boundary layer.

3. Governing equations

Consider a three-dimensional boundary-layer flow and let $U_{\rm ref}$ and $L_{\rm ref}$ be a representative speed and length, respectively; the Reynolds number is defined as $Re = U_{\rm ref} L_{\rm ref}/\nu$, where ν is the kinematic viscosity. In dimensionless variables, the Reynolds-averaged boundary-layer equations in a general orthogonal curvilinear coordinate system are

$$\frac{\partial}{\partial x_1}(h_2 u_1)+\frac{\partial}{\partial x_2}(h_1 u_2)+h_1 h_2 \frac{\partial u_3}{\partial x_3}=0, \tag{3.1}$$

$$\frac{u_1}{h_1}\frac{\partial u_1}{\partial x_1}+\frac{u_2}{h_2}\frac{\partial u_1}{\partial x_2}+u_3\frac{\partial u_1}{\partial x_3}-K_2 u_1 u_2+K_1 u_2^2=-\frac{1}{h_1}\frac{\partial p_{\rm e}}{\partial x_1}+\frac{\partial \tau_{13}}{\partial x_3}, \tag{3.2}$$

$$\frac{u_1}{h_1}\frac{\partial u_2}{\partial x_1}+\frac{u_2}{h_2}\frac{\partial u_2}{\partial x_2}+u_3\frac{\partial u_2}{\partial x_3}-K_1 u_1 u_2+K_2 u_1^2=-\frac{1}{h_2}\frac{\partial p_{\rm e}}{\partial x_2}+\frac{\partial \tau_{23}}{\partial x_3}. \tag{3.3}$$

Here (x_1, x_2) are coordinates in the plane of the wall, x_3 measures the distance normal to the wall, and u_i is the velocity in the x_i direction; $p_{\rm e}(x_1, x_2)$ denotes the mainstream pressure distribution. Furthermore, h_1 and h_2 are the metric coefficients, and K_1 and K_2 are the curvatures defined by

$$K_1=-\frac{1}{h_1 h_2}\frac{\partial h_2}{\partial x_1}, \quad K_2=-\frac{1}{h_1 h_2}\frac{\partial h_1}{\partial x_2}. \tag{3.4a, b}$$

In accordance with conventional boundary-layer theory (Nash & Patel 1972), the metric coefficient in the normal direction h_3 is taken equal to unity and h_1 and h_2 are

assumed independent of x_3. Finally, τ_{13} and τ_{23} are the total shear stresses in the x_1 and x_2 directions, respectively, and are given by

$$\tau_{i3} = s_{i3} + \frac{1}{Re}\frac{\partial u_i}{\partial x_3}, \quad i = 1, 2. \tag{3.5}$$

Here σ_{i3} are the dimensionless Reynolds stresses defined in the usual way (see, for example, Hinze 1975) in terms of time averages of the products of the fluctuating velocities and which in general must be modelled.

Let $(U_{1e}, U_{2e}, 0)$ denote the limiting velocity distribution of the external inviscid flow near the surface ($x_3 \to 0$). A streamline coordinate system is adopted in which x_1 and x_2 are coordinates along and perpendicular to streamlines at the boundary-layer edge, respectively. In this system,

$$U_{1e} = U_e(x_1, x_2), \quad U_{2e} = 0, \tag{3.6a, b}$$

where U_e is the flow speed along the external streamlines near the surface. Therefore, as the boundary-layer edge is approached, $u_1 \to U_e$ and $u_2 \to 0$, and hence the streamwise and cross-stream pressure-gradient terms in (3.2) and (3.3) can be replaced by

$$\frac{1}{h_1}\frac{\partial p_e}{\partial x_1} = -\frac{U_e}{h_1}\frac{\partial U_e}{\partial x_1}, \quad \frac{1}{h_2}\frac{\partial p_e}{\partial x_2} = -K_2 U_e^2, \tag{3.7a, b}$$

respectively. For a given external flow field, the metric coefficients may be obtained as follows. Assuming that the component of vorticity normal to the surface is zero,

$$\frac{\partial}{\partial x_1}(h_2 U_{2e}) = \frac{\partial}{\partial x_2}(h_1 U_{1e}). \tag{3.8}$$

Because U_{2e} is zero everywhere, $h_1 = C_1/U_e$, where C_1 is a scaling factor which may be set to unity without loss of generality. To obtain the second metric coefficient, h_2, first define a function $q(x_1, x_2)$ such that

$$qU_e = \operatorname*{Lim}_{x_3 \to 0} \frac{\partial U_{3e}}{\partial x_3}, \tag{3.9}$$

where U_{3e} denotes the normal velocity distribution in the external flow. The continuity equation (3.1) at the boundary-layer edge becomes

$$\frac{\partial}{\partial x_1}(h_2 U_e) + h_1 h_2 q U_e = 0, \tag{3.10}$$

or, upon using (3.4a), it follows that

$$K_1 = -\frac{1}{h_1 h_2}\frac{\partial h_2}{\partial x_1} = \frac{1}{U_e h_1}\frac{\partial U_e}{\partial x_1} + q. \tag{3.11}$$

Equation (3.11) defines a differential equation for h_2 which may be integrated along individual streamlines. For the special case of $q = 0$ (corresponding to inviscid flows which are effectively independent of x_3 near the surface) a solution of (3.11) is $h_2 = U_e^{-1}$.

To obtain the governing equations along the plane of symmetry, $x_2 = 0$, it may be noted that all quantities appearing in (3.1)–(3.3) are even functions in x_2, with the exception of u_2, K_2, τ_{23} and σ_{23}, which are odd in x_2. Consequently, expanding each

term in (3.1)–(3.3) in a Taylor series about $x_2 = 0$ and retaining only the leading-order terms, the governing equations for the plane of symmetry may be shown to be

$$\frac{\partial}{\partial x_1}(h_2 u_1) + h_1 h_2 u_2' + h_1 h_2 \frac{\partial u_3}{\partial x_3} = 0, \tag{3.12}$$

$$\frac{u_1}{h_1}\frac{\partial u_1}{\partial x_1} + u_3 \frac{\partial u_1}{\partial x_3} = \frac{U_e}{h_1}\frac{\partial U_e}{\partial x_1} + \frac{\partial \tau_{13}}{\partial x_3}, \tag{3.13}$$

$$\frac{u_1}{h_1}\frac{\partial u_2'}{\partial x_1} + u_2'^2 + u_3 \frac{\partial u_2'}{\partial x_3} - 2K_1 u_1 u_2' - K_2'(U_e^2 - u_1^2) = \frac{\partial \tau_{23}'}{\partial x_3}, \tag{3.14}$$

where the primes denote the following quantities evaluated at $x_2 = 0$:

$$u_2' = \frac{1}{h_2}\frac{\partial u_2}{\partial x_2}, \quad K_2' = \frac{1}{h_2}\frac{\partial K_2}{\partial x_2} = -\frac{1}{h_1 h_2^2}\frac{\partial^2 h_1}{\partial x_2^2}, \tag{3.15a, b}$$

$$\sigma_{23}' = \frac{1}{h_2}\frac{\partial \sigma_{23}}{\partial x_2}, \quad \tau_{23}' = \frac{1}{h_2}\frac{\partial \tau_{23}}{\partial x_2} = \sigma_{23}' + \frac{1}{Re}\frac{\partial u_2'}{\partial x_3}. \tag{3.16a, b}$$

At an x_2 location off the plane of symmetry, the unprimed quantities are related to their primed counterparts by

$$u_2 = x_2 h_2 u_2' + O(x_2^3), \quad K_2 = x_2 h_2 K_2' + O(x_2^3), \tag{3.17a, b}$$

$$\sigma_{23} = x_2 h_2 \sigma_{23}' + O(x_2^3), \quad \tau_{23} = x_2 h_2 \tau_{23}' + O(x_2^3). \tag{3.18a, b}$$

The above equations are exact in the plane of symmetry but accurate to $O(x_2^2)$ near the plane of symmetry. The boundary conditions are given by

$$u_1 = u_2' = u_3 = 0 \quad \text{at} \quad x_3 = 0, \tag{3.19}$$

and

$$u_1 \to U_e, \quad u_2' \to 0, \tag{3.20}$$

at the boundary-layer edge.

4. The asymptotic structure in the limit of large Reynolds number

The two-dimensional turbulent boundary layer has a self-consistent two-layer structure in the limit of $Re \to \infty$, which has been described by a number of authors (Yajnik 1970; Fendell 1972; Mellor 1972). A similar but more complicated structure is expected for three-dimensional boundary layers. For a plane of symmetry, it is observed from (3.13) that the streamwise momentum equation is similar to that in two-dimensional flow apart from the change in the normal velocity u_3 due to u_2' in (3.12). This suggests that the structure for the two-dimensional problem should carry over to the plane of symmetry to leading order. However, it emerges that the symmetry-plane problem is more complex and the analysis must be completed through two orders to obtain physically meaningful results for the cross-stream velocity distribution. A brief outline of the main ideas used to obtain the gauge functions will be presented here and a more detailed development is given elsewhere (Degani 1991).

First some important nomenclature is introduced. Let u_τ denote the dimensionless friction velocity defined in the usual way as

$$u_\tau = \tau_w^{\frac{1}{2}}, \tag{4.1}$$

where τ_w is the dimensionless wall shear stress. Next, by definition, the wall skew angle θ_w is given by

$$\tan\theta_w = \tau_{23}/\tau_{13} \quad \text{at} \quad x_3 = 0. \tag{4.2}$$

A Taylor series expansion of θ_w about the plane of symmetry defined by $x_2 = 0$ gives

$$\theta_w = x_2 h_2 \theta_w' + O(x_2^3), \quad \theta_w' = \frac{1}{h_2}\frac{\partial\theta_w}{\partial x_2}\bigg|_{x_2=0}. \tag{4.3a, b}$$

Consequently, substitution of (3.18*b*) and (4.3*a*) into (4.2) and evaluating the resultant expression at $x_2 = 0$ yields

$$\theta_w' = \tau_{23}'/\tau_{13} \quad \text{at} \quad x_3 = 0. \tag{4.4}$$

Finally, there are two pressure-gradient parameters relevant to the present study and these are defined according to

$$\beta_s = \frac{\Delta_0}{U_e u_\tau}\frac{1}{h_1}\frac{\partial p_e}{\partial x_1}, \quad \beta_n = \frac{\Delta_0}{U_e u_\tau}\frac{1}{h_2}\frac{\partial p_e}{\partial x_2}, \tag{4.5a, b}$$

where the pressure gradients are given by (3.7). Here Δ_0 is a function representative of the boundary-layer thickness and is of $O(u_\tau)$ (Fendell 1972). The function β_n vanishes at $x_2 = 0$; however, with the use of (3.7*b*) and (3.17*b*), a Taylor series expansion of β_n yields

$$\beta_n = x_2 h_2 \beta_n' + O(x_2^3), \quad \beta_n' = -\frac{\Delta_0 K_2' U_e}{u_\tau}, \tag{4.6a, b}$$

where β_n' is in general non-zero along the symmetry plane.

The asymptotic analysis is taken up now. First, consider known results for the leading-order streamwise problem. The Reynolds and total shear stresses are $O(u_\tau^2)$ throughout the boundary layer, while the leading-order terms for streamwise velocity in the outer and inner layers are of the form (Fendell 1972; Walker *et al.* 1989)

$$u_1 = U_e(x_1) + u_\tau(x_1; Re)\frac{\partial F_1}{\partial\eta}(x_1, \eta) + \ldots, \tag{4.7a}$$

$$u_1 = u_\tau(x_1; Re)\, U^+(y^+) + \ldots, \tag{4.7b}$$

respectively. The scaled outer and inner variables are defined by

$$\eta = x_3/\Delta_0, \quad y^+ = x_3/\Delta_1, \quad \Delta_1 = (Re\, u_\tau)^{-1}, \tag{4.8a–c}$$

where the conventional definition of y^+ has been used. In the overlap zone, both profile functions in (4.7) behave logarithmically (Fendell 1972) according to

$$\frac{\partial F_1}{\partial\eta} \sim \frac{1}{\kappa}\log\eta + C_0 \quad \text{as} \quad \eta \to 0, \tag{4.9a}$$

and

$$U^+ \sim \frac{1}{\kappa}\log y^+ + C_1 \quad \text{as} \quad y^+ \to \infty. \tag{4.9b}$$

Here κ is the von Kármán constant and C_1 is the inner-region log-law constant which are often assumed to have universal values of 0.41 and 5.0, respectively; C_0 is a

function of x_1 which is determined, in general, from a numerical solution for $\partial F_1/\partial\eta$. Matching of the velocities in (4.7) and using (4.9) yields the match condition

$$\frac{U_e}{u_\tau} = \frac{1}{\kappa}\log(Re\, u_\tau \Delta_0) + C_i - C_0, \tag{4.10}$$

which relates u_τ to the Reynolds number and the outer thickness Δ_0. It is noted in passing that it follows from (4.10) that u_τ is $O(1/\log Re)$ to leading order.

The primary balance within the wall layer is between the Reynolds and viscous shear stresses since the pressure-gradient and convective terms are of higher relative order. Thus, (3.13) reduces to $\partial\tau_{13}/\partial x_3 = 0$, and as a result the total shear stress in the wall layer is constant to leading order and equal to the value at the wall, viz.

$$\tau_{13} = u_\tau^2. \tag{4.11}$$

Since the viscous stress is expected to be small for large y^+, (4.11) establishes the order of magnitude of the Reynolds stress; hence

$$\sigma_{13} = u_\tau^2 \sigma_1(y^+) + \dots . \tag{4.12}$$

Substitution of (4.7*b*), (4.8), (4.11) and (4.12) into (3.5) yields

$$\frac{dU^+}{dy^+} + \sigma_1 = 1, \tag{4.13}$$

which is the mathematical statement that the sum of viscous and Reynolds stresses is constant in the wall layer. In view of (4.11), the total shear stress in the outer layer is expanded according to

$$\tau_{13} = u_\tau^2 T_1(x_1, \eta) + \dots, \tag{4.14}$$

where

$$T_1 \to 1 \quad \text{as} \quad \eta \to 0. \tag{4.15}$$

Note that the expansion (4.14) reflects a somewhat different approach for the outer layer from that adopted by Fendell (1972) as described by Degani (1991).

The first-order results are well-known and the objective now is to develop the next terms in the expansions. To this end, consider first the streamwise momentum equation in the wall layer. Upon substituting (4.7*b*) into (3.13) and using (4.8*c*), it may be shown that

$$\frac{\partial\tau_{13}}{\partial y^+} = -\frac{1}{Re\, u_\tau}\frac{U_e}{h_1}\frac{\partial U_e}{\partial x_1} + \frac{u_\tau}{Re}\left\{\frac{1}{U_e h_1}\frac{\partial U_e}{\partial x_1}(U^+)^2 + K_1\frac{dU^+}{dy^+}\int_0^{y^+} U^+\, dy^+\right\} + \dots \tag{4.16}$$

to leading order. Integration of the above equation from $y^+ = 0$ and subsequent evaluation for large y^+ yields the asymptotic form of τ_{13} at the wall-layer edge, viz.

$$\tau_{13} = u_\tau^2 - \frac{1}{Re\, u_\tau}\frac{U_e}{h_1}\frac{\partial U_e}{\partial x_1}y^+ + \frac{u_\tau}{Re}\frac{1}{U_e h_1}\frac{\partial U_e}{\partial x_1}\frac{y^+\log^2 y^+}{\kappa^2} + \dots \quad \text{as} \quad y^+ \to \infty. \tag{4.17}$$

The first term in (4.17) matches the outer-layer expansion (4.14) as $\eta \to 0$ but, to complete the matching, higher-order terms are required in the expansion for τ_{13} in the outer layer. The form of (4.17) suggests the following extension of the expansion (4.14):

$$\tau_{13} = u_\tau^2 T_1(x_1, \eta) + \frac{u_\tau^3}{U_e} T_2(x_1, \eta) + \dots . \tag{4.18}$$

It can be verified that in order to match the shear stress in the outer layer to the asymptotic form in (4.17), T_1 and T_2 are required to behave according to

$$T_1 \sim 1 - \frac{2\beta_s}{\kappa}\eta\log\eta + \ldots, \tag{4.19a}$$

$$T_2 \sim \frac{\beta_s}{\kappa^2}\eta\log^2\eta + \ldots \quad \text{as} \quad \eta \to 0, \tag{4.19b}$$

where β_s is defined by (4.5a). It should be emphasized that a specific turbulence closure has not been made at this stage in the analysis and that (4.19) are valid regardless of the choice of turbulence model.

It may be inferred from (3.13) and (4.18) that in the outer layer, the corresponding expansion for u_1 is of the form

$$u_1 = U_e + u_\tau \frac{\partial F_1}{\partial \eta} + \frac{u_\tau^2}{U_e}\frac{\partial F_2}{\partial \eta} + \ldots . \tag{4.20}$$

The second-order term in (4.20) must vanish for large η and, as discussed below, in this study

$$\frac{\partial F_2}{\partial \eta} \sim C_1 \quad \text{as} \quad \eta \to 0. \tag{4.21}$$

In general, the quantities C_0 and C_1 in (4.9a) and (4.21) are functions of x_1 which are to be found and whose values depend on the specific closure model adopted. The form of (4.21) merits some discussion. If the leading-order term in (4.21) were logarithmic (as is the case in (4.9a)), a term $O(u_\tau^2/U_e)$ would be required as the next term in the expansion (4.7b). But, in the present study, the first term in (4.7b) captures the entire logarithmic structure of the wall layer that would otherwise require an inner expansion in terms of a parameter ϵ which to leading order is $O(u_\tau/U_e)$ (cf. Mellor 1972). This point is discussed in greater detail elsewhere (Degani 1991). Upon matching (4.7b) and (4.20) by using (4.9) and (4.21), it may be easily confirmed that the match condition (4.10) up to second order now reads

$$\frac{U_e}{u_\tau} = \frac{1}{\kappa}\log(Re\, u_\tau \Delta_0) + C_1 - C_0 - \frac{u_\tau}{U_e}C_1 + \ldots . \tag{4.22}$$

The leading-order expansions given here are in accordance with past analyses (Yajnik 1970; Fendell 1972; Mellor 1972); however, there are significant differences in the higher-order terms which merit some discussion. In the conventional approach used by Mellor (1972) and Melnik (1981), the wall-layer velocity and outer-layer defect function are expanded in a power series of a small parameter ϵ which is $O(1/\log Re)$. The parameter ϵ is taken to be independent of x_1 with $\epsilon \to 0$ as $Re \to \infty$ (see also Neish & Smith 1988). Substitution of a power series in ϵ for the inner-layer expansions into the momentum equation then leads to the conclusion that the total shear stress in the wall layer is a constant to all orders in ϵ and consequently the pressure gradient does not influence the wall-layer flow. Using this expansion scheme, a similar conclusion was reached by Goldberg & Reshotko (1984) for three-dimensional boundary layers. However, a difficulty with this expansion procedure is that it is not capable of including the effects of pressure gradient. The present analysis follows Fendell's (1972) approach where the x_1 and Re dependence is contained implicitly in the expansion parameters u_τ and Δ_0.

The cross-stream problem is somewhat subtle and the asymptotic structure for this aspect will now be addressed. In the outer layer, u_2' is expected to be comparable to the streamwise defect velocity, i.e. $O(u_\tau)$; therefore, in the outer layer let

$$u_2' = u_\tau(x_1; Re)\,\theta_*'(x_1; Re)\frac{\partial G_1}{\partial \eta}(x_1, \eta) + \ldots, \tag{4.23}$$

to leading order. Here θ_*' is $O(1)$ and will subsequently be shown to be proportional to θ_w'. At the boundary-layer edge, $\partial G_1/\partial\eta \to 0$, but as η decreases within the outer layer, u_2' is expected to increase in magnitude under the influence of the cross-stream pressure gradient. However, $\partial G_1/\partial\eta$ cannot behave logarithmically as $\eta \to 0$ since the wall layer cannot adjust a function which is logarithmic to leading order to zero at the wall; thus $\partial G_1/\partial\eta$ is expected to be $O(1)$ for small η. To confirm that this is the case, consider first the form of (3.14) in the wall layer. The orders of magnitude of u_2' and τ_{23}' have not been determined at this stage but are expected to be at most $O(u_\tau)$ and $O(u_\tau^2)$, respectively. Thus, the convection and cross-stream pressure-gradient terms on the left-hand side of (3.14) are expected to be at most $O(u_\tau^2)$ and $O(1)$ and, therefore, negligible with respect to the total stress gradient. Consequently, to leading order in the wall layer,

$$\partial\tau_{23}'/\partial y^+ = 0. \tag{4.24}$$

This result is supported by the scalings subsequently derived for the cross-stream wall-layer flow. Thus τ_{23}' is a constant to leading order in the wall layer and equal to its value at the wall. Consequently, from (4.4) and (4.11),

$$\tau_{23}' = \theta_w' u_\tau^2. \tag{4.25}$$

Following arguments similar to those associated with the streamwise problem, expand the cross-stream Reynolds stress and u_2' in the wall layer according to

$$\sigma_{23}' = \theta_w' u_\tau^2 \tilde{\sigma}_1(y^+) + \ldots, \quad u_2' = \theta_w' u_\tau \Omega^+(y^+) + \ldots, \tag{4.26}$$

where $\tilde{\sigma}_1$ and Ω^+ are to be found. Using the (3.16*b*) and (4.25), along with (4.8*c*), the governing equation in the wall layer to leading order in the cross-stream direction is

$$\frac{\mathrm{d}\Omega^+}{\mathrm{d}y^+} + \tilde{\sigma}_1 = 1. \tag{4.27}$$

From (4.13), the above equation is identically satisfied if

$$\Omega^+(y^+) = U^+(y^+), \quad \tilde{\sigma}_1(y^+) = \sigma_1(y^+). \tag{4.28a, b}$$

This implies that the flow in the wall layer is collateral to leading order, a result previously obtained by Goldberg & Reshotko (1984).

It follows from (4.26) and (4.28) and the asymptotic condition (4.9*b*) that

$$u_2' \sim \theta_w' u_\tau \left\{\frac{1}{\kappa}\log y^+ + C_1\right\} \quad \text{as} \quad y^+ \to \infty. \tag{4.29}$$

Using (4.8) and the match condition (4.10), it is easily shown that in the outer layer,

$$u_2' \sim \theta_w' U_e + \theta_w' u_\tau \left\{\frac{1}{\kappa}\log\eta + C_0\right\} \quad \text{as} \quad \eta \to 0, \tag{4.30}$$

which supports the argument behind (4.23), and gives

$$\theta_w' = (u_\tau/U_e)\,\theta_*'. \tag{4.31}$$

Since the quantity θ'_*, which was introduced in (4.23), is $O(1)$, an important result of the present analysis is that θ'_w is $O(u_\tau/U_e)$ or alternatively, from (4.3a), the skew angle at the wall $\theta_w \sim O(u_\tau/U_e)$ for a fixed x_2 location off the plane of symmetry.

The appropriate expansion for the cross-stream velocity in the outer layer is inferred by substituting (4.31) into (4.30) and is given by

$$u'_2 = u_\tau \theta'_* \frac{\partial G_1}{\partial \eta} + \frac{u_\tau^2 \theta'_*}{U_e} \frac{\partial G_2}{\partial \eta} + \ldots, \tag{4.32}$$

subject to conditions

$$\frac{\partial G_1}{\partial \eta} \to 1, \quad \frac{\partial G_2}{\partial \eta} \to \frac{1}{\kappa} \log \eta + C_0 \quad \text{as} \quad \eta \to 0. \tag{4.33a, b}$$

In addition, at the mainstream

$$\frac{\partial G_1}{\partial \eta}, \quad \frac{\partial G_2}{\partial \eta} \to 0 \quad \text{as} \quad \eta \to \infty. \tag{4.34}$$

In the wall layer the leading-order terms for Reynolds stress and u'_2 are obtained by substituting (4.31) into (4.26); this results in

$$\sigma'_{23} = \frac{u_\tau^3}{U_e} \theta'_* \sigma_1(y^+), \quad u'_2 = \frac{u_\tau^2}{U_e} \theta'_* U^+(y^+), \tag{4.35a, b}$$

and it is important to note that σ'_{23} and u'_2 are smaller than their streamwise counterparts in the wall layer by an amount $O(u_\tau/U_e)$. With the leading-order terms determined in the wall layer, (4.24) is confirmed.

At this stage, it is worthwhile to discuss how the cross-stream velocity attains the characteristic profile 'bulge'. In the outer part of the boundary layer, that is at η-locations above the maximum cross-stream velocity, u'_2 is dominated by the first-order term, i.e. the term $O(u_\tau)$ in (4.32). As η decreases to zero, the first-order term increases and asymptotes towards $u_\tau \theta'_*$. However, as η decreases towards zero, the logarithm in the second-order term in (4.32) eventually begins to contribute significantly and reduces the sum of the $O(u_\tau)$ and $O(u_\tau^2/U_e)$ terms to $O(u_\tau^2/U_e)$, in much the same fashion as the sum of the external velocity U_e and the defect function reduces the streamwise velocity to $O(u_\tau)$ in the wall layer; this represents that part of the profile below the η-location of the maximum cross-stream velocity where both terms in (4.32) are significant. Therefore, the 'bulge' in the cross-stream velocity profile is a natural consequence of the asymptotic structure; this result is in contrast to Goldberg & Reshotko (1984) who adopted an empirical formula to obtain the desired profile shape in the cross-stream direction.

The form of the higher-order terms in the cross-stream momentum equation is addressed now. It is easily shown from (3.14) that

$$\frac{\partial \tau'_{23}}{\partial y^+} = -\frac{1}{Re\, u_\tau} K'_2 U_e^2 + \frac{u_\tau}{Re} K'_2 \{U^+(y^+)\}^2 + \ldots. \tag{4.36}$$

Integration of this equation from $y^+ = 0$ and subsequent evaluation for large y^+ yields

$$\tau'_{23} \sim \frac{u_\tau^3}{U_e} \theta'_* - \frac{1}{Re\, u_\tau} K'_2 U_e^2 y^+ + \frac{u_\tau}{Re} K'_2 \frac{y^+ \log^2 y^+}{\kappa^2} + \ldots \quad \text{as} \quad y^+ \to \infty. \tag{4.37}$$

This suggests that the cross-stream total shear stress in the outer layer has the following expansion (cf. (4.17) and (4.18)):

$$\tau'_{23} = u_\tau^2 \theta'_* \tilde{T}_1(x_1, \eta) + \frac{u_\tau^3}{U_e} \theta'_* \tilde{T}_2(x_1, \eta) + \ldots, \tag{4.38}$$

where the functions $\tilde{T}_1$ and $\tilde{T}_2$ are required to behave according to

$$\tilde{T}_1 \sim \frac{2\gamma}{\kappa} \eta \log \eta + \ldots, \tag{4.39a}$$

$$\tilde{T}_2 \sim 1 + \frac{\gamma}{\kappa^2} \eta \log^2 \eta + \ldots \quad \text{as} \quad \eta \to 0, \tag{4.39b}$$

in order to match the asymptotic form in (4.37). Here, γ is defined according to

$$\gamma = -\beta'_n / \theta'_*, \tag{4.40}$$

where β'_n is defined in (4.6). Once again, the asymptotic forms given in (4.39) are independent of any specific turbulence model.

5. Outer-layer similarity equations

Self-similar flows have historically been of interest as useful special cases of more general types of boundary layers. Self-similarity implies that the velocity distributions, when appropriately scaled by local flow conditions, become independent of the streamwise coordinate x_1. Such solutions will be obtained here as an illustration of an application of the present analysis as well as to motivate a discussion of some general features of the profiles. For a two-dimensional flow, self-similar velocity profiles in the outer region depend only on the streamwise pressure-gradient parameter β_s defined by (4.5*a*) (see, for example, Fendell 1972). For the plane of symmetry, the cross-stream parameter β'_n, defined in (4.6*b*), comes into play. A family of self-similar solutions in the plane of symmetry will subsequently be obtained, which depend solely on the two independent parameters β_s and β'_n.

Defining quantities ψ and ϕ by

$$u_1 = \frac{1}{h_2} \frac{\partial \psi}{\partial x_3}, \quad u'_2 = \frac{1}{h_1} \frac{\partial \phi}{\partial x_3}, \quad \psi = \phi = 0 \quad \text{at} \quad \eta = 0, \tag{5.1}$$

it follows from the continuity equation (3.12) that

$$u_3 = -\frac{1}{h_1 h_2} \frac{\partial \psi}{\partial x_1} - \frac{\phi}{h_1}. \tag{5.2}$$

The asymptotic analysis of §4 indicates that, in the outer layer, ψ and ϕ should be expanded up to second order according to

$$\psi = U_e h_2 \Delta_0 \eta + u_\tau h_2 \Delta_0 F_1(\eta) + \frac{u_\tau^2}{U_e} h_2 \Delta_0 F_2(\eta) + \ldots, \tag{5.3a}$$

$$\phi = u_\tau \theta'_* h_1 \Delta_0 G_1(\eta) + \frac{u_\tau^2}{U_e} \theta'_* h_1 \Delta_0 G_2(\eta) + \ldots. \tag{5.3b}$$

The expansions for the total stresses (in (4.18) and (4.38)) and the functions in (5.3) are to be substituted into (3.13) and (3.14) with the aim of isolating first- and second-

order problems for the profile functions F_i and G_i, $i = 1, 2$. These substitutions give rise to terms involving $\partial u_\tau/\partial x_1$, and an expression for this quantity may be obtained by differentiating the match condition (4.22) and using the fact that C_0 and C_1 must be constant for self-similarity (cf. (4.9*a*) and (4.21)). It is easily verified that

$$\frac{1}{h_1}\frac{\partial u_\tau}{\partial x_1} = \frac{u_*}{h_1}\frac{\partial U_e}{\partial x_1} + u_*^2\frac{u_\tau}{\Delta_0}\frac{(\beta_s - \alpha)}{\kappa} + O(u_*^3), \tag{5.4}$$

where u_* and α are defined by

$$u_* = u_\tau/U_e, \tag{5.5}$$

and

$$\alpha = \frac{U_e}{u_\tau h_1}\frac{\partial \Delta_0}{\partial x_1}, \tag{5.6}$$

and β_s is as defined by (4.5*a*). In addition to the parameters α, β_s and γ (see (4.40)), there are three other parameters which occur in the leading-order equations and these are defined here as follows:

$$\nu = qU_e\Delta_0/u_\tau, \tag{5.7}$$

$$\lambda = U_e\Delta_0\theta'_*/u_\tau, \tag{5.8}$$

$$\delta = \frac{\Delta_0 U_e}{u_\tau}\frac{1}{\theta'_* h_1}\frac{\partial \theta'_*}{\partial x_1}. \tag{5.9}$$

Because the analysis is carried out to second order, it is necessary, in principle, to account for the fact that α, β_s and γ, as well as the parameters defined in (5.7)–(5.9) which are all $O(1)$ to leading order, may have expansions in powers of u_*. However, a convenient choice for Δ_0 will be made subsequently (see (5.20) below) and thus ν and β_s may be considered to be fixed in terms of the outer scale Δ_0 and known mainstream quantities. On the other hand θ'_* is to be determined, and since it is proportional to a scaled angle at the wall (cf. (4.3) and (4.31)), it is expected to involve contributions from both the first- and second-order profiles. Thus γ and λ, as well as the quantities α and δ which contain streamwise gradients of boundary-layer quantities, must generally be expanded as series in u_* according to

$$\alpha = \alpha_0 + u_*\alpha_1 + \ldots, \tag{5.10a}$$

$$\delta = \delta_0 + u_*\delta_1 + \ldots, \tag{5.10b}$$

$$\gamma = \gamma_0 + u_*\gamma_1 + \ldots, \tag{5.10c}$$

$$\lambda = \lambda_0 + u_*\lambda_1 + \ldots, \tag{5.10d}$$

where $\alpha_0, \alpha_1, \delta_0, \delta_1, \gamma_0, \gamma_1, \lambda_0$ are constants to be determined.

With the above definitions, the following leading-order equations are obtained:

$$\frac{dT_1}{d\eta} + (\alpha_0 - \nu)\eta\frac{d^2F_1}{d\eta^2} + 2\beta_s\frac{dF_1}{d\eta} = 0, \tag{5.11}$$

$$\frac{d\tilde{T}_1}{d\eta} + (\alpha_0 - \nu)\eta\frac{d^2G_1}{d\eta^2} + (2\nu - \beta_s - \delta_0)\frac{dG_1}{d\eta} = 2\gamma_0\frac{dF_1}{d\eta}. \tag{5.12}$$

The second-order terms satisfy

$$\frac{dT_2}{d\eta} + (\alpha_0 - \nu)\eta\frac{d^2F_2}{d\eta^2} + 2\beta_s\frac{dF_2}{d\eta} = Z_1(\eta), \tag{5.13}$$

$$\frac{d\tilde{T}_2}{d\eta} + (\alpha_0 - \nu)\eta\frac{d^2G_2}{d\eta^2} + (2\nu - \beta_s - \delta_0)\frac{dG_2}{d\eta} = Z_2(\eta), \tag{5.14}$$

where

$$Z_1(\eta) = -\frac{(\alpha_0-\beta_s)}{\kappa}\frac{dF_1}{d\eta} - \alpha_1\eta\frac{d^2F_1}{d\eta^2} - (\alpha_0-\nu)F_1\frac{d^2F_1}{d\eta^2} - \beta_s\left(\frac{dF_1}{d\eta}\right)^2 - \lambda_0 G_1\frac{d^2F_1}{d\eta^2}, \quad (5.15)$$

and

$$Z_2(\eta) = -\left\{\frac{(\alpha_0-\beta_s)}{\kappa} - \delta_1\right\}\frac{dG_1}{d\eta} - \alpha_1\eta\frac{d^2G_1}{d\eta^2} - (2\nu-\beta_s-\delta_0)\frac{dF_1}{d\eta}\frac{dG_1}{d\eta} - (\alpha_0-\nu)F_1\frac{d^2G_1}{d\eta^2}$$
$$+\lambda_0\left(\frac{dG_1}{d\eta}\right)^2 - \lambda_0 G_1\frac{d^2G_1}{d\eta^2} + \gamma_0\left(\frac{dF_1}{d\eta}\right)^2 + 2\gamma_1\frac{dF_1}{d\eta} + 2\gamma_0\frac{dF_2}{d\eta}. \quad (5.16)$$

Equations (5.11)–(5.16) contain nine parameters α_0, α_1, δ_0, δ_1, β_s, γ_0, γ_1, ν and λ_0 which must all be constants for a similarity solution to be possible; however, these constants are not all independent and connecting relations are now derived.

The streamwise displacement thickness is defined by

$$\delta^* = \int_0^\infty \left\{1 - \frac{u_1}{U_e}\right\} dx_3. \quad (5.17)$$

Upon substituting the expansion for the streamwise velocity given in (4.20) and carrying out the integration, it follows that

$$\delta^* = -\Delta_0\left\{\frac{u_\tau}{U_e}F_{1\infty} + \frac{u_\tau^2}{U_e^2}F_{2\infty} + \ldots\right\}, \quad (5.18)$$

where $F_{i\infty}$ denotes the limit of $F_i(\eta)$ for large η, and the conditions

$$F_1(\eta)\to 0, \quad F_2(\eta)\to 0 \quad \text{as} \quad \eta\to 0, \quad (5.19)$$

have been used. The outer lengthscale Δ_0 is defined (Fendell 1972) according to

$$\Delta_0 = \delta^* U_e/u_\tau, \quad (5.20)$$

and it then follows from (5.18) that

$$F_{1\infty} = -1, \quad F_{2\infty} = 0. \quad (5.21)$$

The streamwise and cross-stream pressure-gradient parameters, defined by (4.5) become

$$\beta_s = -\frac{\delta^*}{u_\tau^2}\frac{U_e}{h_1}\frac{\partial U_e}{\partial x_1}, \quad \beta_n = -\frac{\delta^*}{u_\tau^2}K_2 U_e^2, \quad (5.22a)$$

and from (4.6*b*),

$$\beta_n' = -\frac{\delta^*}{u_\tau^2}K_2' U_e^2. \quad (5.22b)$$

Thus β_s is equivalent to the Clauser parameter defined in connection with self-similar two-dimensional turbulent boundary layers (Mellor & Gibson 1966). Similarly, ν, γ and λ may all be written in terms of δ^*.

An integral of the first-order streamwise equation (5.11) is readily obtained (Fendell 1972). Using the boundary conditions

$$T_1\to 1; \quad \eta\frac{dF_1}{d\eta}, F_1\to 0 \quad \text{as} \quad \eta\to 0, \qquad T_1, \eta\frac{dF_1}{d\eta}\to 0; \quad F_1\to -1 \quad \text{as} \quad \eta\to\infty, \quad (5.23)$$

integration of (5.11) across the boundary-layer thickness yields

$$\alpha_0 = 1+\nu+2\beta_s, \tag{5.24}$$

determining α_0 for a given ν and β_s.

Next, since λ_0 and λ_1 must be constant for similarity, it follows from (5.4) and (5.10*d*) that $\mathrm{d}\lambda/\mathrm{d}x_1$ is $O(u_*^2)$. Upon differentiation of (5.8) and with subsequent use of (5.6), (5.9) and the definition of β_s, it may be shown that

$$\delta = -\alpha - u_* \frac{(\alpha-\beta_s)}{\kappa} + O(u_*^2). \tag{5.25}$$

Therefore, from (5.10),

$$\delta_0 = -\alpha_0, \quad \delta_1 = -\left\{\alpha_1 + \frac{(\alpha_0-\beta_s)}{\kappa}\right\}. \tag{5.26}$$

An expression for α_1 is derived by integrating the second-order streamwise equation in a manner similar to that for the first-order equation. Using the boundary conditions

$$T_2 \to 0; \quad \eta \frac{\mathrm{d}F_2}{\mathrm{d}\eta}, F_2 \to 0 \quad \text{as} \quad \eta \to 0, \qquad T_2 \to 0; \quad \eta \frac{\mathrm{d}F_2}{\mathrm{d}\eta}, F_2 \to 0 \quad \text{as} \quad \eta \to \infty, \tag{5.27}$$

integration of (5.13) across the boundary-layer thickness yields

$$\alpha_1 = \frac{(1+\nu+\beta_s)}{\kappa} + (1+\beta_s) S_{ff} + \lambda_0 S_{fg}, \tag{5.28}$$

where

$$S_{ff} = \int_0^\infty \frac{\mathrm{d}F_1}{\mathrm{d}\eta}\frac{\mathrm{d}F_1}{\mathrm{d}\eta}\mathrm{d}\eta, \quad S_{fg} = \int_0^\infty \frac{\mathrm{d}F_1}{\mathrm{d}\eta}\frac{\mathrm{d}G_1}{\mathrm{d}\eta}\mathrm{d}\eta. \tag{5.29}$$

Both of these constants may be evaluated once the first-order profiles are known. Note that the conditions on F_2 at the boundary-layer edge (i.e. as $\eta \to \infty$) in (5.27) require modification when an interaction with the external flow is accounted for (Neish & Smith 1988).

Next, define a quantity σ according to

$$\sigma = \Delta_0 U_e / u_\tau, \tag{5.30}$$

and upon using (5.4), it is easily shown that

$$\frac{1}{h_1}\frac{\partial \sigma}{\partial x_1} = \alpha_0 + O(u_*). \tag{5.31}$$

Note that by definition σ is always positive. It has been shown elsewhere (Degani 1991) that $\alpha_0 = 0$ corresponds to a degenerate case of a two-dimensional flow, and for brevity this case is not considered here. If s measures distance along the plane of symmetry, then $\mathrm{d}s = h_1 \mathrm{d}x_1$ and for $\alpha_0 \neq 0$ integration of (5.31) yields

$$\sigma = \alpha_0 (s - s_0) \tag{5.32}$$

to leading order, where s_0 is the constant of integration. Using the definitions of β_s and ν along with (3.11), it is evident that

$$\frac{1}{U_e h_1}\frac{\partial U_e}{\partial x_1} = -\frac{\beta_s}{\sigma}, \quad K_1 = -\frac{1}{h_1 h_2}\frac{\partial h_2}{\partial x_1} = \frac{\nu-\beta_s}{\sigma}. \tag{5.33}$$

Upon using (5.32) and noting that $\mathrm{d}s = h_1\,\mathrm{d}x_1$ along the plane of symmetry, integration of (5.33) yields

$$U_e = U_0|s-s_0|^{-\beta_s/\alpha_0}, \quad h_2 = h_{20}|s-s_0|^{(\beta_s-\nu)/\alpha_0}, \tag{5.34a, b}$$

where U_0 and h_{20} are constants along $x_2 = 0$. Note that (5.34a) is the usual power-law dependence associated with self-similarity. Also, from the definitions of λ, γ, σ and β'_n, it follows that $K'_2 = \lambda\gamma/\sigma^2$ and, consequently, from (5.10) and (5.32),

$$K'_2 = \frac{\lambda_0\gamma_0}{\alpha_0^2(s-s_0)^2} \tag{5.35}$$

to leading order. The cross-stream pressure gradient is then obtained using (4.6), (5.30), (5.32), (5.34) and (5.35) and is given by

$$\beta_n = -x_2\frac{h_{20}\lambda_0\gamma_0}{|\alpha_0|}|s-s_0|^{(\beta_s-\nu-\alpha_0)/\alpha_0}, \tag{5.36}$$

since σ is positive.

We henceforth consider a specific class of solutions in which β_n is constant along individual streamlines adjacent to the plane of symmetry. Since $x_2 =$ constant defines the equation of a streamline, then for β_n to be independent of s, (5.36) implies that $\nu = -\alpha_0+\beta_s$. This result when combined with (5.24) yields

$$\nu = -\tfrac{1}{2}(1+\beta_s), \quad \alpha_0 = \tfrac{1}{2}(1+3\beta_s). \tag{5.37}$$

Upon defining a constant β'_{n0} by

$$\beta'_{n0} = \beta_n/(x_2 h_{20}), \tag{5.38}$$

and combining (5.36) and (5.37), it follows that

$$\lambda_0 = -\beta'_{n0}\frac{|1+3\beta_s|}{2\gamma_0}. \tag{5.39}$$

It is assumed here that the cross-stream pressure gradient is given in the form in (5.38) and therefore β'_{n0} is known. It may be shown (Degani 1991) that γ_0 and γ_1 (also C_0 and C_1) are obtained as part of the numerical solution of (5.11)–(5.16). Consequently, with (5.26), (5.28), (5.37) and (5.39), the similarity equations contain only two pressure-gradient parameters β_s and β'_{n0} thus forming a two-parameter family of similarity solutions as anticipated earlier. Note that although β'_{n0} does not appear in the similarity equations, it does so implicitly through (5.39). Finally, from (5.8), (5.10d), (5.30), (5.32) and (5.37), the scaled skew angle at the wall is given by

$$\theta'_* = \frac{2\lambda_0}{(1+3\beta_s)(s-s_0)} \tag{5.40}$$

to leading order.

6. Turbulence closure and similarity solutions

The asymptotic results obtained in §4 are independent of any turbulence model; however, in order to obtain solutions of the similarity equations (5.11)–(5.16), a specific turbulence model must be adopted. Here, simple eddy-viscosity formulae for the outer layer defined by

$$\tau_{13} = \epsilon_1\frac{\partial u_1}{\partial x_3}, \quad \tau'_{23} = \epsilon_2\frac{\partial u'_2}{\partial x_3}, \tag{6.1a, b}$$

are used for illustrative purposes. Here ϵ_1 and ϵ_2 are the total (turbulent + kinematic) viscosities in the streamwise and cross-stream directions. Although an asymptotic analysis cannot achieve closure, it does constrain the possible forms allowable for ϵ_1 and ϵ_2. To this end, consider first the streamwise flow. Substituting the outer-layer asymptotic expansions for the total shear stress and velocity given by (4.18) and (4.20), respectively, into (6.1*a*) and using the definition of Δ_0 given by (5.20), it is seen that

$$T_1 + u_* T_2 = \frac{\epsilon_1}{U_e \delta^*} \left\{ \frac{\partial^2 F_1}{\partial \eta^2} + u_* \frac{\partial^2 F_2}{\partial \eta^2} \right\}, \tag{6.2}$$

where u_* is defined by (5.5). The simplest turbulence model is obtained by representing ϵ_1 as a single term so that

$$T_1 = \frac{\epsilon_1}{U_e \delta^*} \frac{\partial^2 F_1}{\partial \eta^2}, \quad T_2 = \frac{\epsilon_1}{U_e \delta^*} \frac{\partial^2 F_2}{\partial \eta^2}. \tag{6.3a, b}$$

In order to obtain the behaviour indicated in (4.9*a*) and (4.19*a*), (6.3*a*) implies that

$$\epsilon_1 \sim U_e \delta^* \kappa \eta + \ldots \quad \text{as} \quad \eta \to 0, \tag{6.4}$$

which fixes the form of ϵ_1 for small η. Consequently a simple outer-layer model given by

$$\epsilon_1 = U_e \delta^* \epsilon_m, \tag{6.5}$$

where

$$\epsilon_m = \begin{cases} K, & \eta \geqslant K/\kappa, \\ \kappa \eta, & \eta < K/\kappa \end{cases} \tag{6.6}$$

is asymptotically consistent. Here κ is the von Kármán constant and K is an empirically determined constant. The model described by (6.5) and (6.6) is similar to that used by Mellor & Gibson (1966) for two-dimensional boundary layers with $K = 0.016$. Now consider the cross-stream flow. Introducing the outer-layer expansions (4.32) and (4.38) into (6.1*b*) and representing ϵ_2 by a single term results in

$$\tilde{T}_1 = \frac{\epsilon_2}{U_e \delta^*} \frac{\partial^2 G_1}{\partial \eta^2}, \quad \tilde{T}_2 = \frac{\epsilon_2}{U_e \delta^*} \frac{\partial^2 G_2}{\partial \eta^2}, \tag{6.7}$$

which establishes the scale of ϵ_2 as identical to that of ϵ_1. From (4.33*b*) and (4.39*b*), it follows that

$$\epsilon_2 \sim U_e \delta^* \kappa \eta + \ldots \quad \text{as} \quad \eta \to 0, \tag{6.8}$$

and, consequently, a cross-stream model given by

$$\epsilon_2 = U_e \delta^* \epsilon_m \tag{6.9}$$

is also asymptotically consistent. The model described by (6.5) and (6.9) is essentially similar to a class of turbulence models currently used to compute numerical solutions of three-dimensional turbulent flows (Cebeci 1975; Wie & DeJarnette 1988). The model is often referred to as isotropic since the same behaviour is assumed in both the streamwise and cross-stream directions.

In two-dimensional turbulent boundary layers, the velocity, velocity-gradient and the Reynolds stress vectors all lie in the same plane; however, for three-dimensional boundary layers, experiments show that the Reynolds stress vector and velocity-

gradient vectors do not coincide in general. Consequently, it follows that the eddy viscosities for the streamwise and cross-stream directions must be different and thus the eddy viscosity is said to be non-isotropic. Johnston (1976), using data from four experiments, remarked that the ratio of the cross-stream to streamwise eddy viscosity was in the range 0.2 to 1.0. Similar results have been quoted recently by Anderson & Eaton (1987). However, other experiments (see, for example, Fernholz & Vagt 1981; Muller 1982*a*) have indicated a ratio of the eddy viscosities of greater than unity. Some researchers (e.g. Muller 1982*b*) have attempted to model this aspect by assuming the ratio ϵ_2/ϵ_1 to be a constant other than unity throughout the thickness of the boundary layer. However, the results summarized by (6.4), (6.8) and (4.28) indicate that the ratio ϵ_2/ϵ_1 must be unity in the logarithmic zone and the wall layer to leading order. Note that eddy-viscosity models which are not isotropic could be introduced in the present formulation in the outer region of the outer layer by adopting a different value of the outer constant K in each of the coordinate directions.

There is some evidence to indicate that an isotropic model for the entire boundary layer is appropriate for self-similar flow. Johnston (1976) comments that it is only in situations where there are relatively sudden changes in the external cross-stream direction that the direction of the total stress lags that of the velocity gradient substantially; however, as the flow subsequently relaxes downstream and adjusts to new smoother external conditions, the two directions do tend to coincide. Self-similar states are expected to resemble this last condition and hence the model in (6.5) and (6.9) is considered reasonable here. With the model given by (6.5) and (6.9), the shear stress functions in (5.11)–(5.14) are related to the velocity functions by

$$T_i = \epsilon_m \frac{\mathrm{d}^2 F_i}{\mathrm{d}\eta^2}, \quad \tilde{T}_i = \epsilon_m \frac{\mathrm{d}^2 G_i}{\mathrm{d}\eta^2}, \quad i = 1, 2. \tag{6.10}$$

Using the model (6.10) and substituting for ν, α_0 and δ_0 from (5.37) and (5.26), the first-order problems (5.11) and (5.12) become

$$(\epsilon_m F_1'')' + (1+2\beta_s)\,\eta F_1'' + 2\beta_s F_1' = 0, \tag{6.11}$$

$$(\epsilon_m G_1'')' + (1+2\beta_s)\,\eta G_1'' - \tfrac{1}{2}(1+\beta_s)\,G_1' = 2\gamma_0 F_1'. \tag{6.12}$$

Here the primes denote differentiation with respect to η. The boundary conditions at the edge of the boundary layer are given by

$$F_1', G_1' \to 0 \quad \text{as} \quad \eta \to \infty, \tag{6.13}$$

and as $\eta \to 0$ by (4.9*a*) and (4.33*a*). A simple analytical solution of (6.11) is readily obtained for the special case $\beta_s = 0$ (Bogucz & Walker 1988), but it is most convenient to obtain a numerical solution of (6.11) for values of $\beta_s \neq 0$. For a given value of β_s, the constant C_0 appearing in (4.9*a*) is determined by following a procedure described by Yuhas & Walker (1982). Furthermore, as described by Degani (1991), a numerical solution of (6.12) produces a value for γ_0. Once γ_0 is determined, the value of λ_0 may be calculated from (5.39) for a given β_{n0}'.

The second-order problems (5.13) and (5.14) are given by

$$(\epsilon_m F_2'')' + (1+2\beta_s)\,\eta F_2'' + 2\beta_s F_2' = Z_1, \tag{6.14}$$

$$(\epsilon_m G_2'')' + (1+2\beta_s)\,\eta G_2'' - \tfrac{1}{2}(1+\beta_s)\,G_2' = Z_2, \tag{6.15}$$

where $$Z_1(\eta) = -\frac{(1+\beta_s)}{2\kappa}F_1' - \alpha_1 \eta F_1'' - (1+2\beta_s)F_1 F_1'' - \beta_s (F_1')^2 - \lambda_0 G_1 F_1'', \tag{6.16}$$

$$Z_2(\eta) = 2\gamma_0 F_2' + 2\gamma_1 F_1' - \left\{\frac{(1+\beta_s)}{\kappa} + \alpha_1\right\} G_1' - \alpha_1 \eta G_1'' + \tfrac{1}{2}(1+\beta_s) F_1 G_1'$$
$$- (1+2\beta_s) F_1 G_1'' + \lambda_0 (G_1')^2 - \lambda_0 G_1 G_1'' + \gamma_0 (F_1')^2, \tag{6.17}$$

and α_1 is as defined in (5.28). The boundary conditions at the boundary-layer edge are given by

$$F_2', G_2' \to 0 \quad \text{as} \quad \eta \to \infty, \tag{6.18}$$

and as $\eta \to 0$ by (4.21) and (4.33*b*). The numerical algorithm to solve (6.11)–(6.18) is not straightforward and is described in detail by Degani (1991). It should be noted, however, that the solution of the second-order problems produces values for C_1 and γ_1.

7. Results and discussion

The outer-layer similarity solutions are considered first. The first- and second-order similarity equations may be solved for specific values of β_s and β_{n0}', which are the independent parameters associated with the streamwise and cross-stream pressure gradients, respectively. It is possible to obtain solutions to (6.11)–(6.18) for a wide range of values of β_s and β_{n0}' but here results for one representative case with

$$\beta_s = 0.25, \quad \beta_{n0}' = -0.2 \tag{7.1}$$

are described. The situation in (7.1) corresponds to a boundary layer subjected to a mild adverse pressure gradient in the streamwise direction and in which the external streamlines are concave upward with the flow diverging from the plane of symmetry. The additional constants associated with the problem are calculated and, to three significant figures,

$$\gamma_0 = 0.111, \quad C_0 = -0.177, \quad \lambda_0 = 1.58, \tag{7.2}$$

$$\gamma_1 = 0.848, \quad C_1 = -3.65. \tag{7.3}$$

In order to compare first- and second-order velocity and shear-stress profiles, it is necessary to introduce a specific value of the Reynolds number. Substitution of the outer-layer lengthscale (5.20) into the match condition (4.22) leads to

$$\frac{1}{u_*} = \frac{U_e}{u_\tau} = \frac{1}{\kappa}\log Re_{\delta^*} + C_1 - C_0 - \frac{u_\tau}{U_e} C_1, \tag{7.4}$$

where $Re_{\delta^*} = Re\, U_e \delta^*$ is the Reynolds number based on the displacement thickness. The first-order match condition is obtained by omitting the last term in (7.4) while the second-order result is obtained by retaining the full relation. With the calculated values of C_0 and C_1 in (7.2) and (7.3), and an inner-layer 'log-law' constant $C_i = 5.0$, the value of u_* can be calculated from (7.4) once Re_{δ^*} is specified. The Reynolds number Re_{δ^*} is chosen to be 50000 here to illustrate typical results, and the results to first and second order are

$$u_* = 0.03168, \quad 0.03156, \tag{7.5}$$

respectively. For this Reynolds number, the second-order correction to u_* is small and for most practical purposes may be ignored.

The similarity profiles for the streamwise and cross-stream velocities as well as the streamwise and cross-stream total shear stresses are presented in figure 2. The streamwise velocity profile to second order is given by

$$\frac{u_1}{U_e} = 1 + u_* \frac{dF_1}{d\eta} + u_*^2 \frac{dF_2}{d\eta}, \tag{7.6}$$

and is plotted in figure 2(*a*) using the second value of u_* in (7.5). The first-order profile is obtained by omitting the last term in (7.6) and using the first value of u_* in (7.5). It is evident from figure 2(*a*) that the first- and second-order solutions are almost indistinguishable, indicating that the first-order expansion captures the essential behaviour of the streamwise velocity profile. This conclusion is similar to that reached by Mellor & Gibson (1966) for two-dimensional equilibrium turbulent boundary layers. The asymptotic logarithmic behaviour for small values of η and the characteristic outer 'wake' profile should be noted in figure 2(*a*). Since the velocity profiles are valid only in the outer layer, they cannot be continued all the way to the wall. In terms of the wall-layer variable y^+, the lower limit of the outer layer was arbitrarily chosen to be $y^+ = 100$. Since the outer variable is related to the wall-layer variable by $\eta = y^+/Re_{\delta^*}$, then for the Reynolds number under consideration, the lower limit of η is given by 0.002. This value of η corresponds to the location at which the plots in figures 2(*a*) and 2(*b*) are terminated.

The cross-stream velocity near the symmetry plane is proportional to u_2' (cf. (3.17*a*)) and the first- and second-order profiles are obtained from

$$\frac{u_2'}{u_\tau \theta_*'} = \frac{dG_1}{d\eta}, \tag{7.7a}$$

and

$$\frac{u_2'}{u_\tau \theta_*'} = \frac{dG_1}{d\eta} + u_* \frac{dG_2}{d\eta}, \tag{7.7b}$$

respectively, where the first-order estimate of u_* was used in (7.7*b*). Unlike the streamwise profile, there is a significant difference between the first- and second-order results. As indicated by the asymptotic results, the first-order profile (7.7*a*) asymptotes to unity in the limit $\eta \to 0$. On the other hand, the cross-stream velocity (7.7*b*), accurate to second-order, increases, reaches a maximum value, and then decreases, thus creating the characteristic 'bulge' in the cross-stream profile. As η decreases further, the velocity asymptotes logarithmically to match the velocity distribution in the wall layer given by (4.35*b*). The difference between the first- and second-order results is most pronounced for small values of η; however, farther away from the wall, the difference between the two profiles is marginal, as expected.

The total streamwise shear stress up to second order is given by

$$\tau_{13}/u_\tau^2 = T_1 + u_* T_2, \tag{7.8}$$

and the first- and second-order profiles are plotted in figure 2(*c*). The first-order profile is obtained by omitting the last term in (7.8) and for the second-order profile, the value of u_* based on the second-order estimate was used in (7.8). Note that the total shear stress, unlike the velocity, is regular as $\eta \to 0$ and thus the profiles in figure 2(*c*) (and figure 2*d*) may be continued all the way to the wall. As was the case with the streamwise velocity, the second-order term produces only a small correction to the first-order result. In subsequent results shown in this paper, the second-order corrections to the streamwise velocity and total shear stress as well as to the scaled

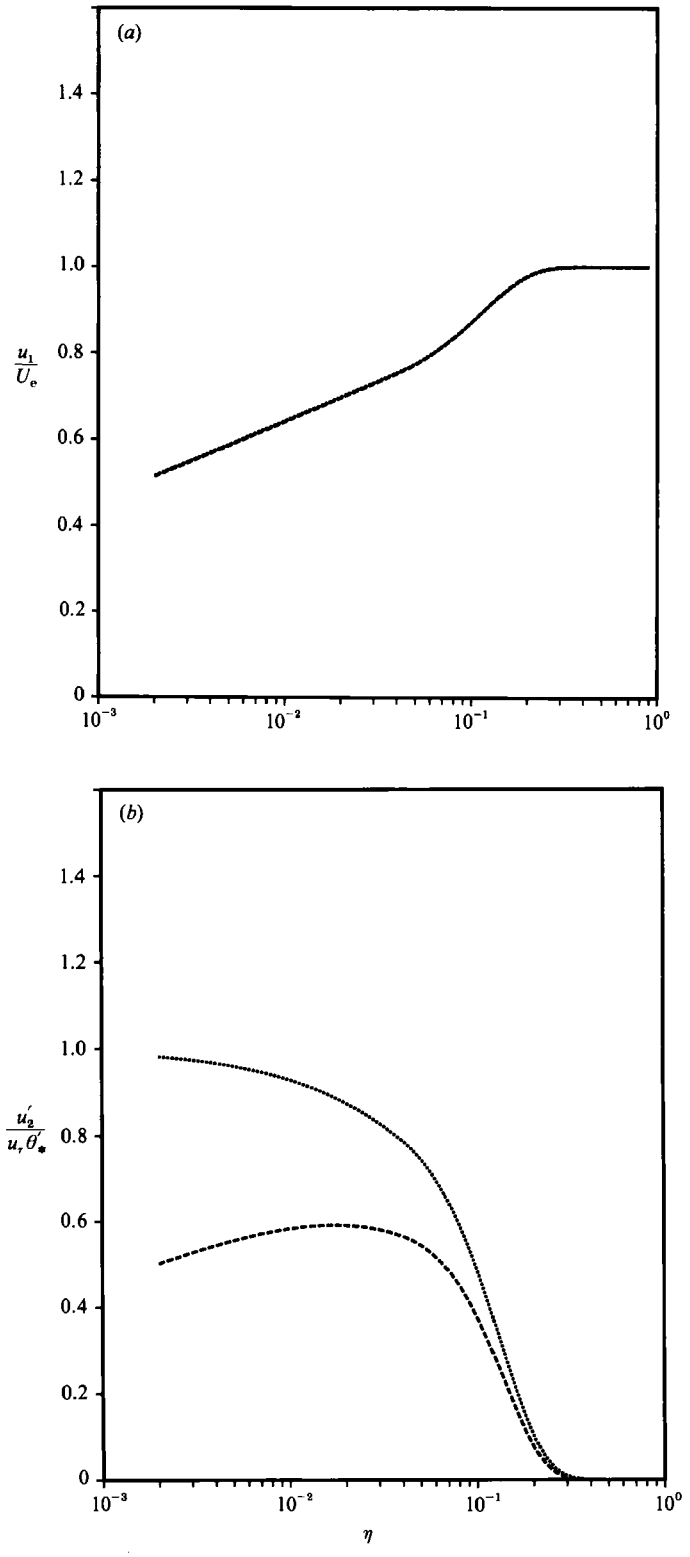

FIGURE 2(*a–b*). For caption see facing page.

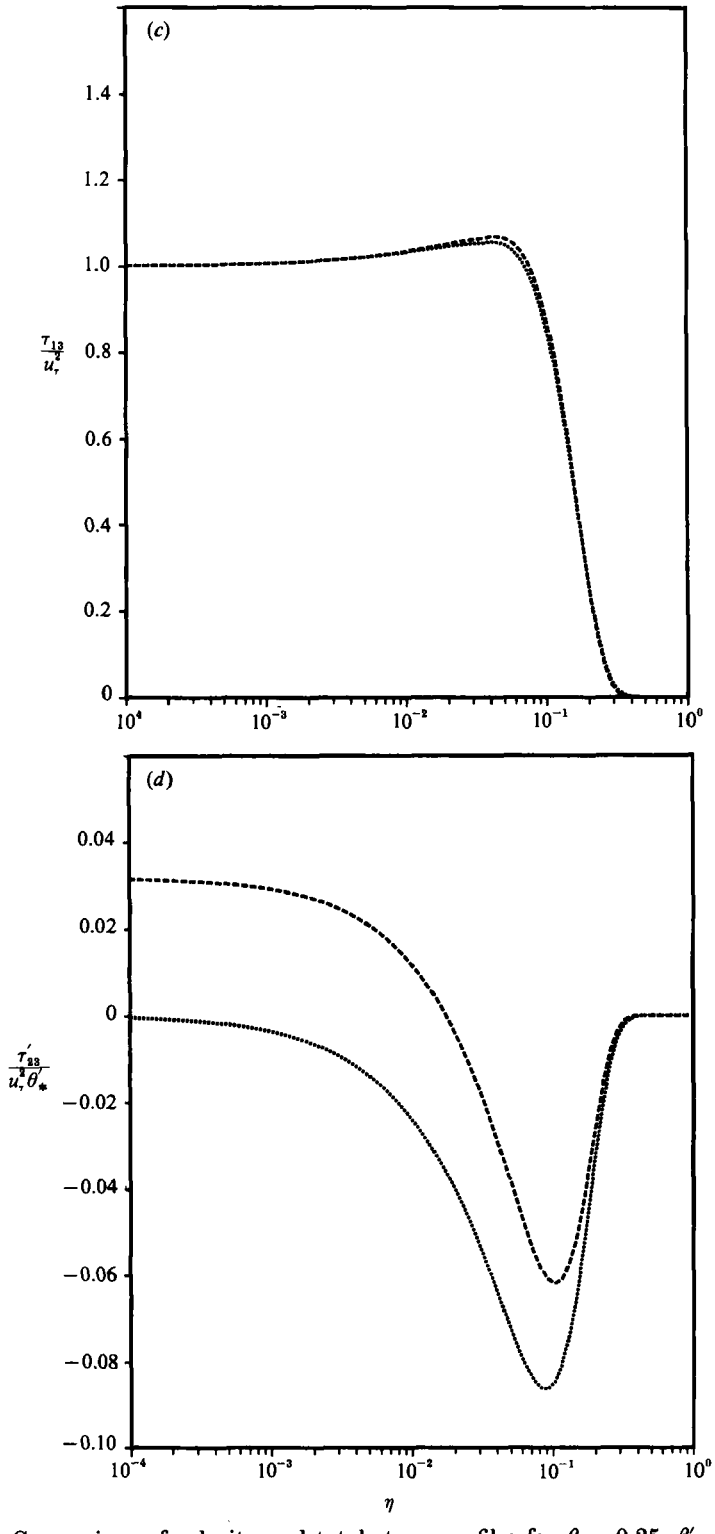

FIGURE 2. Comparison of velocity and total stress profiles for $\beta_s = 0.25$, $\beta'_{n0} = -0.20$ and $Re_{\delta^*} = 50000$: ..... first order, ––– second order. (*a*) Streamwise velocity profile, (*b*) cross-stream velocity profile, (*c*) streamwise total shear stress profile, (*d*) cross-stream total shear stress profile.

friction velocity u_* will be ignored. It is noted in passing that the location of the point of maximum streamwise shear stress occurs within the outer layer in boundary layers subjected to adverse pressure gradients, which is consistent with the results of Mellor & Gibson (1966).

The total cross-stream shear stress up to second order is given by

$$\tau'_{23}/u_\tau^2\theta'_* = \tilde{T}_1 + u_* \tilde{T}_2. \tag{7.9}$$

As was the case with the cross-stream velocity, there is a substantial difference between the first- and second-order results near the wall. Since the cross-stream velocity gradient is positive from the wall to the location of the maximum cross-stream velocity and negative beyond, the shear stress should reflect the same behaviour. The first-order shear stress is obtained by omitting the last term in (7.9) and is seen to be negative throughout; hence it is not sufficient to properly represent the flow. However, the correct trend is obtained from the full second-order profile given by (7.9), being positive close to the wall and negative farther away.

Next, composite profiles across the entire boundary layer for the streamwise and cross-stream velocities are considered. The outer-layer similarity solutions obtained previously must be matched asymptotically to an inner wall-layer solution in order to describe completely the velocities from the wall to the boundary-layer edge. For this to be possible, the function $U^+(y^+)$ appearing in (4.7*b*) and (4.35) must be known and should be such that it satisfies the no-slip condition at the wall and the asymptotic condition in (4.9*b*). One such wall-layer profile for $U^+(y^+)$ has been developed by Walker *et al.* (1989) for two-dimensional turbulent boundary layers and was used in the present study. The profile model $U^+(y^+)$ described by Walker *et al.* (1989) is based upon consideration of the observed coherent structure of the time-dependent wall-layer flow. During the majority of any observation period, the turbulent wall layer is observed to be in a relatively well-ordered or quiescent state (see, for example, Cantwell 1981; Willmarth 1975) when 'low-speed streaks' may be observed. The wall-layer development is interrupted by brief periods of strong interaction with the outer layer in an event usually referred to as 'bursting'; this event is always initiated near a low-speed streak and is characterized by a very localized and abrupt eruption of the wall-layer fluid. Walker *et al.* (1989) considered simplified representative motions in the wall layer during a typical cycle between bursts, and upon time-averaging produced an expression for the mean velocity profile in the wall layer. The expression for $U^+(y^+)$ satisfies the asymptotic condition (4.9*b*) for large y^+ as well as the correct compatibility conditions at the surface, and is given explicitly by Walker *et al.* (1989). It is worthwhile to comment on why this profile model may also be used for the three-dimensional boundary layer. It is reasonably well-established that a dominant feature of the turbulent boundary layer is the hairpin vortex (Smith *et al.* 1990, 1991) and that the observed low-speed streaks are the signature in the wall layer of convected hairpin vortices; furthermore, wall-layer bursting is provoked as a consequence of the adverse pressure gradient induced by the moving hairpin vortex (Walker 1990*a*, *b*; Smith *et al.* 1991). Consequently, in a three-dimensional attached turbulent boundary layer, the hairpin vortices (and the low-speed streaks) will generally be oriented in the local flow direction near the surface. Thus, the time-dependent development of the wall-layer flow will be similar to that in two dimensions, and the profile model of Walker *et al.* (1989) can also be used to describe the mean flow distributions here.

Composite profiles spanning the entire boundary layer can be constructed using the outer-layer solutions given by (7.6) and (7.7) and the wall-layer profiles in (4.7*b*)

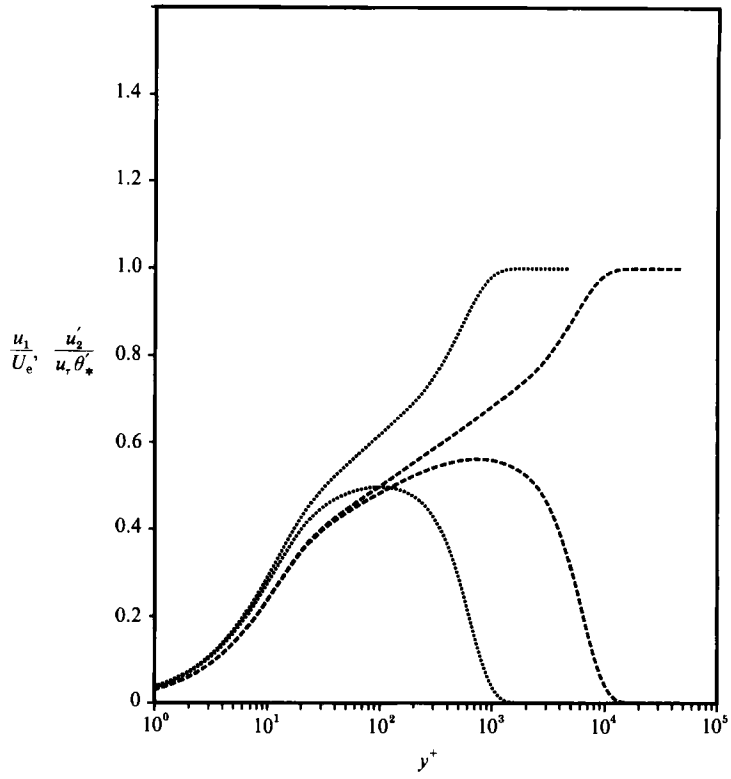

FIGURE 3. The streamwise and cross-stream velocity profiles for $\beta_s = 0.5$, $\beta'_{n0} = -0.20$ at Reynolds numbers of (*a*) ..... $Re_{\delta^*} = 5000$; (*b*) --- $Re_{\delta^*} = 50000$.

and (4.35*b*); in the present study, only terms up to first order were retained in (7.6). The complete streamwise and cross-stream profiles are

$$\frac{u_1}{U_e} = u_* U^+(y^+) + \left\{1 + u_* \frac{dF_1}{d\eta}\right\} - U_c, \tag{7.10a}$$

$$\frac{u_2'}{u_\tau \theta_*'} = u_* U^+(y^+) + \left\{\frac{dG_1}{d\eta} + u_* \frac{dG_2}{d\eta}\right\} - U_c, \tag{7.10b}$$

where U_c denotes the common part given by

$$U_c = u_* \left\{\frac{1}{\kappa} \log y^+ + C_1\right\}, \tag{7.11}$$

in terms of the inner variable y^+; alternatively, using the velocity match condition (4.10), U_c may be expressed in terms of the outer variable η by

$$U_c = 1 + u_* \left\{\frac{1}{\kappa} \log \eta + C_0\right\}. \tag{7.12}$$

For a specified value of Re_{δ^*}, u_* may be calculated from (7.4) and the profiles given by (7.10) can be constructed. The streamwise and cross-stream velocities for two values of the Reynolds number, namely $Re_{\delta^*} = 5000$ ($u_* = 0.0369$) and $Re_{\delta^*} = 50000$ ($u_* = 0.0306$), and the case $\beta_s = 0.5, \beta'_{n0} = -0.20$ are plotted in terms of the inner variable y^+ in figure 3. For the lower Reynolds number, it may be noted that the logarithmic region on either profile does not appear to be well-defined on the graph

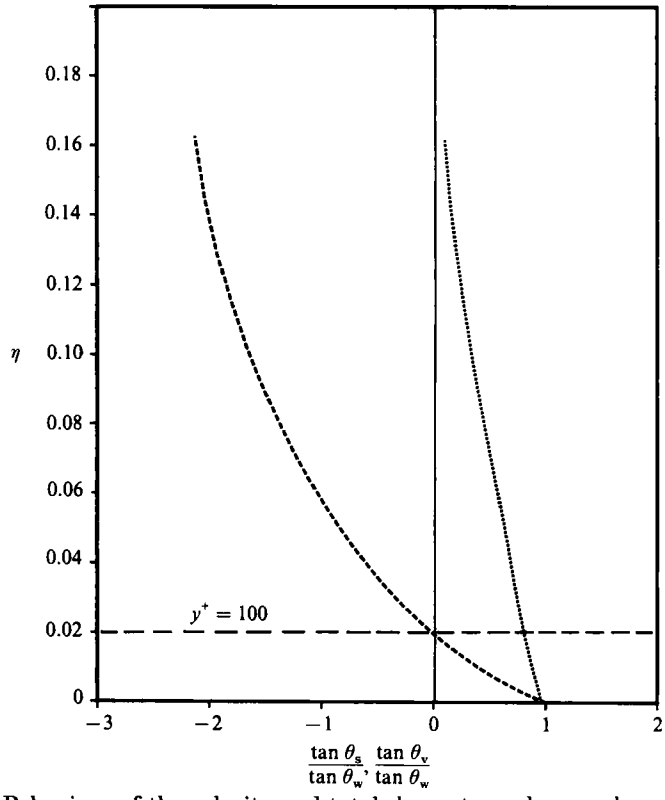

FIGURE 4. Behaviour of the velocity and total shear stress skew angles near the surface for $\beta_s = 0.5$, $\beta'_{n0} = -0.20$ and $Re_{\delta^*} = 5000$: ....., θ_v; ---θ_s.

even though the plotted composite profile explicitly contains the logarithmic variation. Furthermore, the values of the velocities only coincide up to around $y^+ = 5$, indicating that the region of truly collateral flow extends to a very small distance from the wall in terms of y^+. On the other hand, at the higher Reynolds number the logarithmic region is well-defined on the graph for both velocity profiles; the two velocities coincide to around $y^+ = 50$, thus indicating an increasing extent of collateral flow (in terms of y^+) as the Reynolds number increases. This is consistent with the asymptotic analysis presented in §4. The plotted results shown in figure 3 are useful in explaining why the issue of the extent of collateral flow in the wall layer has been controversial, as well as why it has been difficult to discern a logarithmic portion in the cross-stream velocity profile from experimental data obtained at low Reynolds numbers.

The behaviour of the skew angles for the velocity and total shear stress near the wall is shown in figure 4 for $Re_{\delta^*} = 5000$, $\beta_s = 0.5$ and $\beta'_{n0} = -0.2$. Both skew angles must approach the angle at the wall θ_w which is used as a convenient normalization factor. The skew angle for the total shear stress, denoted by θ_s, is plotted in figure 4 and is given by

$$\frac{\tan\theta_s}{\tan\theta_w} = \frac{\tau_{23}/\tau_{13}}{\tan\theta_w}, \tag{7.13}$$

and upon using (4.18), (4.38) along with (3.18) and (4.3), it is easily confirmed that

$$\frac{\tan\theta_s}{\tan\theta_w} = \frac{1}{u_*}\frac{(\tilde{T}_1 + u_*\tilde{T}_2 + \ldots)}{(T_1 + u_* T_2 + \ldots)}. \tag{7.14}$$

Because the total shear stress is regular across the wall layer, a composite solution for θ_s is not necessary and (7.14) may be continued to the surface. Since $y^+ = 100$ is usually considered to be near the outer edge of the wall layer, a line corresponding to this location for $Re_{\delta^*} = 5000$ is drawn in figure 4 as a useful point of reference. The velocity skew angle θ_v, also plotted in figure 4, is given by

$$\frac{\tan\theta_v}{\tan\theta_w} = \left(\frac{u_2'}{u_\tau \theta_*'}\right) \Big/ \left(\frac{u_1}{U_e}\right), \tag{7.15}$$

and was evaluated using the composite expansions (7.10). Experimental data on skewing is often presented on the linear scale used in figure 4 and the predicted behaviour, with θ_s varying more rapidly than θ_v near the wall, bears a close similarity to experimental observations (Bradshaw & Pontikos 1985).

It is of interest to examine the issue of skewing near the surface more closely. Using (4.17) and (4.37), along with the definitions of γ and Δ_0 given by (4.40) and (5.20), it can be shown that

$$\frac{\tan\theta_s}{\tan\theta_w} \sim 1 - \frac{\gamma_0 y^+}{Re_{\delta^*} u_*^2} + \ldots, \tag{7.16}$$

to leading order. The second terms in (4.17) and (4.37) represent corrections to the total stresses across the entire wall layer associated with the pressure gradient; thus, it is easily confirmed that the result (7.16) is valid for all y^+. Note that (7.16) is a general result which is independent of any specific turbulence model and furthermore the skewing of the total stress vector near the surface is dependent only on the parameter γ_0, to leading order. For the velocity skew angle, it follows from (4.20), (4.32) and (7.15) that in the outer layer,

$$\frac{\tan\theta_v}{\tan\theta_w} = \frac{G_1' + u_* G_2' + \ldots}{1 + u_* F_1' + \ldots}. \tag{7.17}$$

For the model given by (6.10), it may be confirmed that the asymptotic condition given by (4.9*a*) may be refined to give

$$F_1' \sim \frac{1}{\kappa}\log\eta + C_0 - \frac{2\beta_s}{\kappa^2}\eta\log\eta + \ldots \quad \text{as} \quad \eta \to 0, \tag{7.18}$$

and (4.33) may also be extended to yield

$$G_1' \sim 1 + \frac{2\gamma_0}{\kappa^2}\eta\log\eta + \ldots, \tag{7.19a}$$

$$G_2' \sim \frac{1}{\kappa}\log\eta + C_0 + \frac{\gamma_0}{\kappa^3}\eta\log^2\eta + \ldots \quad \text{as} \quad \eta \to 0. \tag{7.19b}$$

Using (7.18) and (7.19), the limiting form of (7.17) as $\eta \to 0$ may be obtained; upon rewriting the resulting expression in terms of the inner variable, it may be determined that

$$\frac{\tan\theta_v}{\tan\theta_w} \sim 1 - \frac{\gamma_0}{R_{\delta^*} u_*^2}\frac{y^+}{\log y^+} + \ldots \quad \text{as} \quad y^+ \to \infty, \tag{7.20}$$

to leading order. Once again the deviation from collateral flow depends principally on the parameter γ_0. It is evident from (7.16) and (7.20) that the correction to the leading-order collateral flow in the wall layer is $O(\log^2 Re_{\delta^*}/Re_{\delta^*})$, or equivalently

$O(\log^4 Re/Re)$, which approaches zero for large Re; however, for the Reynolds numbers encountered in practice, the correction term is generally not negligible and contributes significantly in altering the collateral behaviour of the near-wall flow. It is seen from figure 4 that at $Re_{\delta^*} = 5000$ both the velocity and total stress vectors do exhibit significant skew angle variation across the wall layer. As Re_{δ^*} increases, the shape of the curves in figure 4 is not noticeably affected, but the line labelled $y^+ = 100$ shifts progressively downward toward the surface, and the wall layer more closely approaches being truly collateral.

It may be noted from (7.16) and (7.20) that the streamwise pressure gradient does not influence the skewing to leading order near the surface. Furthermore, the deviation from collateral flow for the total stress is proportional to y^+, whereas for the velocity it is proportional to $y^+/\log y^+$ at the edge of the wall layer, suggesting that the total stress skews more rapidly than the velocity with the approach to the surface, a result which is confirmed by experimental data (see, for example, Bradshaw & Pontikos 1985). Further comments on the skew angle profiles are given in Degani (1991).

Finally, as an additional example, computed results for the cross-flow velocity profile for $\beta_s = 0$ and increasing values of the cross-stream pressure-gradient parameter are presented; the Reynolds number is arbitrarily fixed at $Re_{\delta^*} = 10000$. The parameters computed from the numerical solutions are given in table 1; for each case $\gamma_0 = 0.095$ and $C_0 = 0.961$, and the first-order value of u_* was calculated to be 0.037 73. The composite profiles obtained from (7.10*b*) are shown in figure 4(*a*), where it may be observed that all four profiles appear to collapse onto one curve. Note that the cross-stream velocity normalized as in (7.10*b*) is independent of the value of the cross-stream pressure-gradient parameter (cf. (5.39), (5.40), (6.11) and (6.12)) to leading order. Consequently, the computed results in figure 5(*a*) indicate that the effect of a change in the value of β'_{n0} in the second-order equations (6.14) and (6.15) is negligibly small for the parameter range considered in table 1. The results in figure 5(*a*) are replotted in figure 5(*b*) with an alternative normalization for u'_2 given by

$$\frac{u'_2}{U_e}|s-s_0| = -\frac{\beta'_{n0}}{\gamma_0}u_*\left\{u_* U^+(y^+) + \left\{\frac{dG_1}{d\eta} + u_*\frac{dG_2}{d\eta}\right\} - U_c\right\}, \tag{7.21}$$

where (7.21) is obtained by substituting (5.5), (5.39), and (5.40) into (7.10*b*). The profile function (7.21) is representative of the actual cross-stream velocity attained in physical space since $u_2 = x_2 h_2 u'_2$. As expected, figure 5(*b*) shows that the cross-stream velocity increases with increasing magnitude of the cross-stream pressure gradient.

8. Conclusions

The theory presented in this paper for turbulent boundary layers near a plane of symmetry is an important step towards an analysis of the full three-dimensional equations; however, the theory is informative in its own right, providing an insight into the nature of the structure of boundary layers in and around the plane of symmetry. Since the full three-dimensional profiles for velocity and shear stress must match smoothly to the profiles obtained here as the plane of symmetry is approached, it is expected that the structure of the three-dimensional boundary layers will be similar. The asymptotic analysis shows that the streamwise profile is affected by the cross-stream flow only in the second order; hence, to leading order, the streamwise profile is identical to that in two-dimensional turbulent boundary

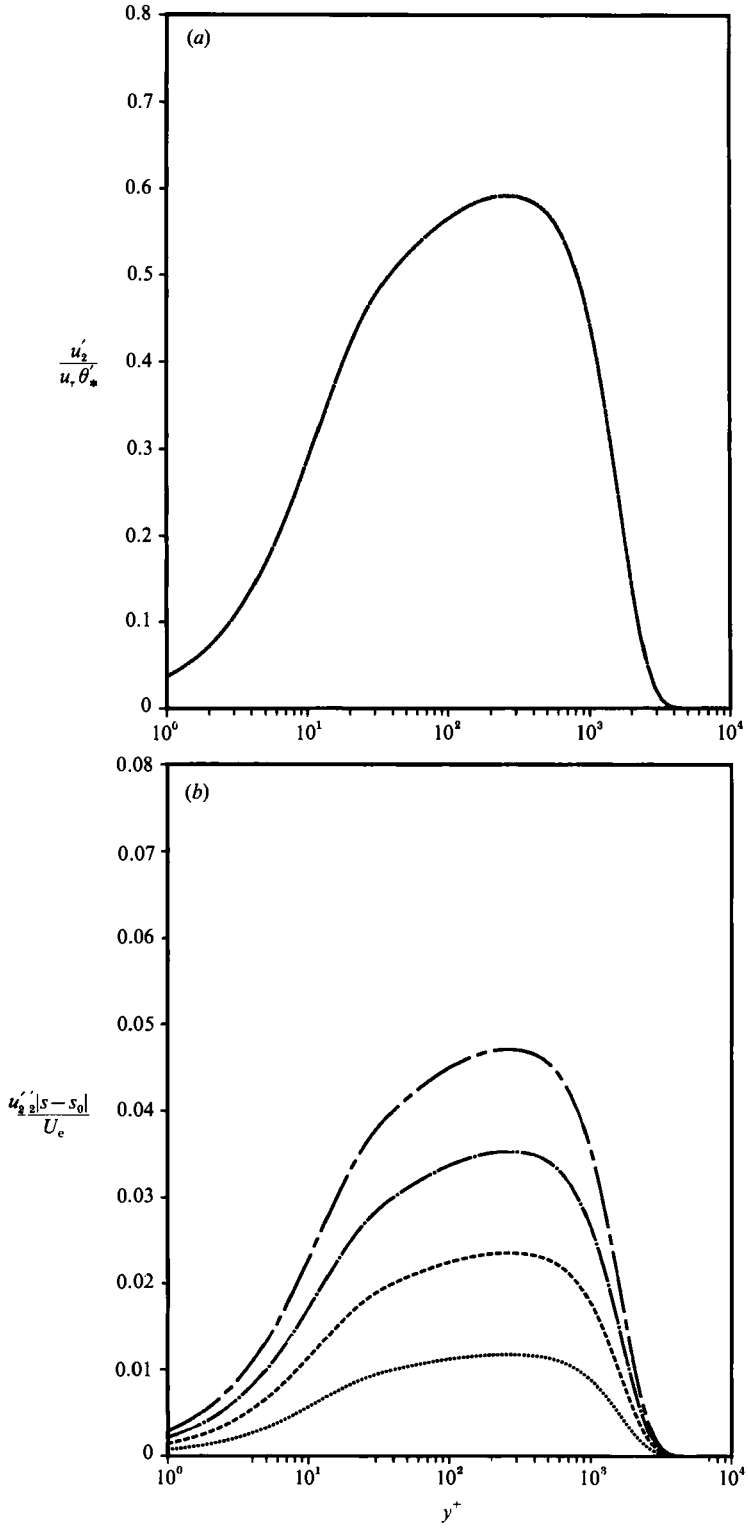

FIGURE 5. Effect of the cross-stream pressure gradient on the cross-stream velocity profile for $\beta_s = 0$ and $Re_{\delta^*} = 10000$: ..... $\beta'_{n0} = -0.05$; --- $\beta'_{n0} = -0.1$; —·— $\beta'_{n0} = -0.15$; ———— $\beta'_{n0} = -0.2$. (*a*) With the normalization of (7.10*b*), (*b*) with the normalization of (7.21).

Profile	β'_{n0}	λ_0	C_1	γ_1
1	−0.05	0.264	−7.79	−0.585
2	−0.1	0.527	−7.71	−0.563
3	−0.15	0.791	−7.64	−0.542
4	−0.2	1.05	−7.56	−0.521

TABLE 1. Values of the parameters for four calculated profiles

layers. The importance of the present analysis, however, lies in the asymptotic structure obtained for the cross-stream velocity profile; it has been shown that the outer-layer cross-stream velocity is not logarithmic to leading order, but is logarithmic in the second order for small η and that within this structure the characteristic 'bulge' in the velocity profile develops. Furthermore, as a consequence of the outer-layer structure, it has been shown that the skew angle at the wall scales on the friction velocity. The flow in the inner layer is collateral only to leading order; furthermore, the second-order effects of pressure gradient are, in general, not negligible and will cause the velocity and shear stress profiles to skew significantly at Reynolds numbers encountered in engineering practice.

A two-parameter family of similarity solutions was determined which is dependent on streamwise and cross-stream pressure-gradient parameters. Similarity solutions for the outer layer were obtained by using a simple turbulence-closure model consistent with the results of the asymptotic analysis. These solutions were then matched asymptotically to an analytical inner-layer profile. It was shown that the extent of collateral flow in the near-wall region, measured in terms of the wall variable y^+, increased with increasing Reynolds number. Furthermore, the logarithmic behaviour for the cross-stream velocity was not apparent graphically at low Reynolds numbers, but became clearly defined at higher values; this probably explains why a logarithmic behaviour of the cross-stream profile has not been discerned in experimental data obtained at low Reynolds number.

The authors gratefully acknowledge the support of NASA Lewis Research Center under grant NAG 3-771 and the Air Force Office of Scientic Research under grant AFOSR-89-0487.

REFERENCES

ANDERSON, S. D. & EATON, J. K. 1987 An experimental investigation of pressure driven three-dimensional turbulent boundary layers. *Rep.* MD-49. Stanford University.

BALDWIN, B. S. & LOMAX, H. 1978 Thin layer approximation and algebraic model for separated turbulent flows. *AIAA 16th Aerosciences Meeting, Huntsville, Alabama, Jan. 16–18.*

BARNWELL, R. W. 1991 Nonadiabatic and three-dimensional effects in compressible turbulent boundary layers. *29th Aerospace Sciences Meeting, Reno, Nevada, AIAA*-91-0528.

BOGUCZ, E. A. & WALKER, J. D. A. 1988 The turbulent near wake at a sharp trailing edge. *J. Fluid Mech.* **196**, 555–584.

BRADSHAW, P. & PONTIKOS, N. S. 1985 Measurements in the turbulent boundary layer on an infinite swept wing. *J. Fluid Mech.* **159**, 105–130.

CANTWELL, B. J. 1981 Organized motion in turbulent flow. *Ann. Rev. Fluid Mech.* **13**, 457–515.

CEBECI, T. 1975 Calculation of three-dimensional boundary layers II. Three-dimensional flow in Cartesian coordinates. *AIAA J.* **13**, 1056–1064.

CEBECI, T. & SMITH, A. M. O. 1974 *Analysis of Turbulent Boundary Layers.* Academic.

CHANDRASEKHAR, N. & SWAMY, N. V. C. 1976 Wall shear stress inference for three-dimensional turbulent boundary layer profiles. *Trans. ASME* E: *J. Appl. Mech.* **43**, 20–27.

CLAUSER, F. H. 1954 Turbulent boundary layers in adverse pressure gradients. *J. Aeronaut. Sci.* **21**, 91–108.

CLAUSER, F. H. 1956 The turbulent boundary layers. In *Advances in Applied Mechanics*, Vol. 4 (ed. Dryden, H. L. & von Kármán, T.), pp. 1–51. Academic.

DEGANI, A. T. 1991 The three-dimensional turbulent boundary layer – theory and application. Ph.D. thesis, Lehigh University.

FENDELL, F. E. 1972 Singular perturbation and turbulent shear flow near walls. *J. Astronaut. Sci.* **20**, 129–165.

FERNHOLZ, H. H. & VAGT, J.-D. 1981 Turbulence measurements in an adverse-pressure-gradient three-dimensional turbulent boundary layer along a circular cylinder. *J. Fluid Mech.* **111**, 233–269.

FRANCIS, G. P. & PIERCE, F. J. 1967 An experimental study of skewed turbulent boundary layers in low speed flows. *Trans. ASME* D: *J. Basic Engng* **89**, 597–607.

GOLDBERG, U. & RESHOTKO, E. 1984 Scaling and modeling of three-dimensional pressure-driven turbulent boundary layers. *AIAA J.* **22**, 914–920.

HEBBAR, K. S. & MELNIK, W. L. 1978 Wall region of a relaxing three-dimensional incompressible turbulent boundary layer. *J. Fluid Mech.* **85**, 33–56.

HINZE, J. O. 1975 *Turbulence*. McGraw-Hill.

HORNUNG, H. G. & JOUBERT, P. N. 1963 The mean velocity profile in three-dimensional turbulent boundary layers. *J. Fluid Mech.* **15**, 368–384.

JOHNSTON, J. P. 1960 On three-dimensional turbulent boundary layers generated by secondary flow. *Trans. ASME* D: *J. Basic Engng* **82**, 233–246.

JOHNSTON, J. P. 1976 Experimental studies in three-dimensional turbulent boundary layers. *Viscous Flow Symp., Lockheed-Georgia Co., June 22–23.*

KLINKSIEK, W. F. & PIERCE, F. J. 1970 Simultaneous lateral skewing in a three-dimensional turbulent boundary layer flow. *Trans. ASME* D: *J. Basic Engng* **92**, 83–90.

MELLOR, G. L. 1972 The large Reynolds number, asymptotic theory of turbulent boundary layers. *Intl J. Engng Sci.* **10**, 851–873.

MELLOR, G. L. & GIBSON, D. M. 1966 Equilibrium turbulent boundary layers. *J. Fluid Mech.* **24**, 225–253.

MELNIK, R. E. 1981 Turbulent interactions on airfoils at transonic speeds – recent developments. In *Computation of Viscous-Inviscid Interactions*, *AGARD*-CP-291, Chap. 10.

MULLER, U. R. 1982*a* Measurement of the Reynolds stresses and the mean-flow field in a three-dimensional pressure-driven boundary layer. *J. Fluid Mech.* **119**, 121–153.

MULLER, U. R. 1982*b* Comparison of three-dimensional turbulent boundary-layer calculations with experiment. *IUTAM Symp. on Three-Dimensional Boundary Layers, Trondheim, Norway.*

NASH, J. F. & PATEL, V. C. 1972 *Three-Dimensional Turbulent Boundary Layers*. SBC Technical Book, Atlanta.

NEISH, A. & SMITH, F. T. 1988 The turbulent boundary layer and wake of an aligned flat plate. *J. Engng Maths* **22**, 15–42.

PIERCE, F. J., MCALLISTER, J. E. & TENNANT, M. H. 1983 A review of near-wall similarity models in three-dimensional turbulent boundary layers. *Trans. ASME* I: *J. Fluids Engng* **105**, 251–262.

PIERCE, F. J. & ZIMMERMAN, B. B. 1973 Wall shear stress inference from two- and three-dimensional turbulent boundary layer velocity profiles. *Trans. ASME* I: *J. Fluids Engng* **95**, 61–67.

PRAHLAD, T. S. 1973 Mean velocity profiles in three-dimensional incompressible turbulent boundary layers. *AIAA J.* **11**, 359–365.

SMITH, C. R., WALKER, J. D. A., HAIDARI, A. H. & SOBRUN, U. 1991 On the dynamics of near-wall turbulence. *Phil. Trans. R. Soc. Lond.* A **336**, 131–175.

SMITH, C. R., WALKER, J. D. A., HAIDARI, A. H. & TAYLOR, B. K. 1990 Hairpin vortices in turbulent boundary layers: the implications for reducing drag. In *Structure of Turbulence and Drag Reduction* (ed. A. Gyr), pp. 51–58. Springer.

VAN DEN BERG, B. 1975 A three-dimensional law of the wall for turbulent shear flows. *J. Fluid Mech.* **70**, 149–160.

VAN DEN BERG, B., ELSENAAR, A., LINDHOUT, J. P. F. & WESSELING, P. 1975 Measurements in an incompressible three-dimensional turbulent boundary layer, under infinite swept-wing conditions, and comparison with theory. *J. Fluid Mech.* **70**, 127–147.

VAN DYKE, M. 1964 *Perturbation Methods in Fluid Mechanics.* Academic.

WALKER, J. D. A. 1990*a* Wall layer eruptions in turbulent flows. In *Structure of Turbulence and Drag Reduction* (ed. A. Gyr), pp. 109–118. Springer.

WALKER, J. D. A. 1990*b* Models based on dynamical features of the wall layer. *Appl. Mech. Rev.* **43**, S232–S239.

WALKER, J. D. A., ABBOTT, D. E., SCHARNHORST, R. K. & WEIGAND, G. G. 1989 A wall-layer model for the velocity profile in turbulent flows. *AIAA J.* **27**, 140–149.

WIE, Y.-S. & DEJARNETTE, F. R. 1988 Numerical investigation of three-dimensional flow separation using the boundary layer equations. *AIAA Paper* 88-0617.

WILLMARTH, W. W. 1975 Structure of turbulence in boundary layers. *Adv. Appl. Mech.* **1**, 159–254.

YAJNIK, K. S. 1970 Asymptotic theory of turbulent shear flows. *J. Fluid Mech.* **42**, 411–427.

YUHAS, L. J. & WALKER, J. D. A. 1982 An optimization technique for the development of two-dimensional steady turbulent boundary-layer models. *Rep.* FM-1, Dept. Mech. Engng and Mechs, Lehigh University; also AFOSR-TR-0417.